PORE DIFFUSION LIMITS REMOVAL OF MONOCHLORAMINE IN TREATMENT OF SWIMMING POOL WATER USING GRANULAR ACTIVATED CARBON

Bertram Skibinski[1*], Christoph Götze[1], Eckhard Worch[2], Wolfgang Uhl[1,3*]

[1] Technische Universität Dresden, Chair of Water Supply Engineering, 01062 Dresden, Germany.

[2] Technische Universität Dresden, Chair of Hydrochemistry, 01062 Dresden, Germany.

[3] Norwegian Institute for Water Research (NIVA), 0349 Oslo, Norway.

[*] Corresponding authors. E-mail address: wolfgang.uhl@niva.no
bertram.skibinski@tu-dresden.de

Key words: swimming pool water; monochloramine; surface catalytic reaction; granular activated carbon; diffusion control

Type of article: Research Paper

Abstract

Overall apparent reaction rates for the removal of monochloramine (MCA) in granular activated carbon (GAC) beds were determined using a fixed-bed reactor system and under conditions typical for swimming pool water treatment. Reaction rates dropped and quasi-stationary conditions were reached quickly. Diffusional mass transport in the pores was shown to be limiting the overall reaction rate. This was reflected consistently in the Thiele modulus, in the effect of temperature, pore size distribution and of grain size on the reaction rates. Pores <2.5 times the diameter of the monochloramine molecule were shown to be barely accessible for the monochloramine conversion reaction. GACs with a significant proportion of large mesopores were found to have the highest overall reactivity for monochloramine removal.

1 Introduction

Hypochlorous acid (HOCl) is widely used as disinfectant in swimming pools due to its effectiveness in disinfection. A major drawback is its reactivity towards inorganic and organic matter present in pool water, which results in the formation of halogenated disinfection by-products (DBPs) (Zwiener et al., 2007; Deborde and von Gunten, 2008).

The dominating nitrogenous precursors for DBP formation that are introduced into the pool by bathers are urea and ammonia (Consolazio et al., 1963). Ammonia reacts with HOCl to progressively form inorganic chloramines (mono-, di- and trichloramine) (Blatchley and Cheng, 2010; Qiang and Adams, 2004). Urea, however, reacts in pool water through progressive chlorine addition forming chlorinated urea, which finally breaks down to form the very volatile trichloramine (Blatchley and Cheng, 2010).

Chloramines are known to be irritating to skin and eyes, and are suspected to cause respiratory problems (Eichelsdörfer et al., 1975). This also includes an increased risk to children of asthma during adolescence (Bernard et al., 2003; Bernard et al., 2008). Consequently, the sum of all inorganic chloramines is strictly regulated to a concentration of <0.2 mg L^{-1} (as Cl_2) in swimming pools in Germany (DIN 19643-2, 2012) and the US (ANSI/APSP-1, 2009). Among the variety of inorganic chloramines, monochloramine (MCA) is the most dominant species in pool water. A study of 11 swimming pools in the US found concentrations of monochloramine of up to 1.88 mg L^{-1} (as Cl_2) (Weaver et al., 2009). Moreover, MCA is particularly of interest because it has been found to be a precursor for the formation of carcinogenic N-nitrosodimethylamine (NDMA) (Schreiber and Mitch, 2006), which was also found in chlorinated pools (Walse and Mitch, 2008).

As bathers are introducing urea and ammonia into swimming pools, the removal of the chloramines formed by the reaction of ammonia can decrease the total concentration of chloramines in the pool. Activated carbons are widely known as effective adsorbents (Worch, 2012; Schreiber et al. 2005). However, previous studies have shown that they are reducing agents for MCA as well. In that, the reduction of MCA primarily proceeds via a surface chemical reaction, and the capacity of granular activated carbon (GAC) filters for MCA removal was found to be higher than expected when only adsorption was considered (Jaguaribe et al., 2005; Bauer and Snoeyink, 1973). Over the course of the reaction, the reactivity of GACs decreased before stationary conditions were reached (Scaramelli and Digiano, 1977). As a result, activated carbon filters operated under swimming pool water conditions have a finite life time and need to be regenerated or replaced after a certain time in operation. However, the exact mechanism of the initial decrease of reactivity has not been fully understood until now. Previous studies proposed a two-step process, where MCA is initially reduced at neutral pH to NH_4^+ at free active carbon sites (C*) (Equation 1). As enough surface oxides were formed, the authors assume that MCA is oxidised to N_2 in a second, slower reaction with surface oxides (Equation 2) (Bauer and Snoeyink, 1973).

$$NH_2Cl + H_2O + C^* \rightarrow NH_4^+ + Cl^- + C^*O \quad (1)$$

$$2\ NH_2Cl + C^*O + H_2O \rightarrow N_2 + 2\ H_3O^+ + 2\ Cl^- + C^* \quad (2)$$

However, a more recent study indicates that the ratio of transformation products (NH_4^+ and N_2) formed did not change over the course of the reaction (Fairey et al. 2007), which contradicts the hypothesis of (Bauer and Snoeyink, 1973). Furthermore, earlier studies reasoned that the overall reactivity is dominated by pore diffusion, rather than by the surface chemical reactions (Komorita and Snoeyink, 1985; Fairey and Speitel, 2006). Mass transport in the pore system of GACs is known to be influenced by various

parameters such as the grain size, water temperature (Ertl et al., 1997), the presence of surface oxides (Mangun et al., 1999) and the pore size distribution of GACs (Maia et al., 2008). To describe theoretically the MCA removal process in GAC filters, the semi-empirical MCA catalysis model (MCAT model) was established by Kim (1977) to predict steady-state MCA removal in GAC filters (Kim, 1977). The MCAT model was complemented recently to take into account the effect of source water type and pH (Fairey and Speitel, 2006). However, the model estimates the GAC reactivity after stationary conditions are reached (Komorita and Snoeyink, 1985) using only basic GAC properties such as the porosity and tortuosity of the GACs. This makes the model inapplicable in elucidating mass transfer effects in detail, which is important when considering the potentials for optimisation of the process.

Thus, considering the current state of knowledge, the process of decreasing reactivity of GACs with increasing reaction time, as well as the impact of pore diffusional limitations on the removal performance of a fixed GAC bed, is still not fully understood. Conclusively, the aim of this study was to determine the impact of diffusional mass transport on the overall MCA removal performance of GAC for a wide range of operation conditions, such as grain size, pore size distribution and water temperature.

2 Materials and Methods

2.1 Fixed bed reactor system for determination of the reaction rate constants

Reaction rate constants for monochloramine removal in GAC beds were determined using the fixed bed reactor (FBR) system shown in Figure 1. It included a glass column of 34 mm inner diameter and a total length of 200 mm, in which the GAC bed is placed on a glass frit. A glass frit close to the inlet ensures equal distribution of the flow to the GAC bed. The GAC bed was continuously fed with an MCA solution at a constant flow rate (Q_{bed}) from a rapidly stirred (~250 rpm), double-walled glass tank of 10 L volume, equipped with a stainless steel lid and with feedback temperature control (B. Braun, Germany). The conductivity of the MCA solution was adjusted to ~400 µS cm^{-1} by dosing 1 mol L^{-1} NaCl solution before the experiment was started. The volumetric flow rate through the bed was maintained by a turbine pump (P1) (BG1-30, Gather Industries, Germany) and was measured using a magnetic inductive flow meter (Altoflux IFM 5080 K with IFC 080 transformer, Krohne, Germany).

The GAC bed was prepared by initially filling the glass column, disconnected from the system, with deionised water. Subsequently, GAC that had been wetted and the pores filled with deionised water by applying a vacuum, was transferred to the column. The bed was then consolidated by carefully tamping the column to guarantee a reproducible packing. After connecting the column to the FBR system, the chloramine solution was circulated through all instruments and tubes while bypassing the column. The experiment was started then by changing the fluid flow from bypass to the GAC bed.

The effluents from the GAC bed or the bypass were fed back to the tank. The MCA concentration in the tank was measured by an amperometric chlorine sensor

(Dulcotest CTE 1 DMT, Prominent, Germany), mounted in a closed loop and flowed through by a peristaltic pump (P2) (5004S, Watson Marlow, UK) at a flow rate of 25 L h^{-1}. The pH in the tank was measured continuously and maintained constant at pH 7, which was in the pH range for swimming pool water (DIN 19643-2, 2012), by dosage with 0.3 mol L^{-1} phosphoric acid or 0.1 mol L^{-1} NaOH using feedback-controlled peristaltic pumps (P4, P5). The level in the tank was kept constant by a peristaltic pump (P3) triggered by a level electrode.

Since MCA was consumed in the GAC bed, the MCA concentration in the tank and thus the MCA inflow concentration to the GAC bed, $c_{bed,in}$, were kept constant by feeding a cooled (4–6 °C) MCA stock solution to the tank using a feedback-controlled peristaltic micro pump (P6) (BVK, Ismatec, Germany). That stock solution was placed on a balance (CA 572, Kern, Germany) and the mass of the stock solution was recorded continuously. Thus, at any time t, the mass flow of stock solution to the tank was known. A SCADA system (TopMessage, Delphin Technologies, Germany) was used for data recording and feedback control of all relevant process parameters of the FBR system.

Figure 1: Scheme of the laboratory-scale FBR system.

2.2 Preparation of the monochloramine stock solution

Monochloramine stock solutions as used in the FBR experiments were prepared by drop-wise addition of 750 mL of a OCl^- solution (pH 10, 0.032 mol L^{-1}, prepared from a sodium hypochlorite solution (>12 % active chlorine)) to 250 mL of a rapidly stirred NH_4Cl or $(NH_4)_2SO_4$ solution (pH 10, 0.098 mol L^{-1} (NH_4Cl) or 0.049 mol L^{-1} ($(NH_4)_2SO_4$)) at a final molar chlorine-to-ammonia ratio of 1.00:1.03 (Aoki, 1989). All chemicals were p.a. reagent grade.

2.3 Analytical quantification of monochloramine and HOCl

The total chlorine sensor of the FBR system was calibrated daily using the spectrophotometric DPD method (DIN EN ISO 7393-2), using a Unicam UV2-200 UV/VIS spectrophotometer with a 5 cm quartz cuvette.

The concentration of the OCl^- solution used to prepare the MCA stock solution was determined spectrophotometrically using a molar absorption coefficient at 294 nm ($\varepsilon_{OCl^-, 294nm}$) of 348 mol^{-1} cm^{-1} (Hand and Magerum, 1983).

The MCA stock solution was determined at least twice a day according to the spectrophotometric method of Schreiber and Mitch, accounting for the overlapping absorbance peaks of MCA and dichloramine ($NHCl_2$) at 245 nm and 295 nm ($\varepsilon_{NH2Cl,\ 245\ nm}$ = 445 mol^{-1} cm^{-1}, $\varepsilon_{NHCl2,\ 245\ nm}$ = 208 mol^{-1} cm^{-1}, $\varepsilon_{NH2Cl,\ 295\ nm}$ = 14 mol^{-1} cm^{-1}, $\varepsilon_{NHCl2,\ 295\ nm}$ = 267 mol^{-1} cm^{-1}) (Schreiber and Mitch, 2005). Measurements at 360 nm confirmed the absence of trichloramine (NCl_3) in the MCA stock solution ($\varepsilon_{NCl3,\ 360\ nm}$ = 126 mol^{-1} cm^{-1}) (Schurter et al., 1995). The yield for transformation of NH_4^+-N to MCA-N was found to be in a range from 95 to 100 %.

2.4 Granular activated carbons

Four commercially available granular activated carbons (GACs) were used in this study, namely Hydraffin 30 N from Donau Carbon GmbH (30 N), Silcarbon K-835 from Silcarbon Aktivkohle GmbH (K835), Centaur from Chemviron Carbon GmbH (Centaur) and a spherically shaped activated carbon Type 100058 from Blücher GmbH (100058). The raw materials of the carbons were anthracite coal (30N), coconut shells (K835), bituminous coal (Centaur) and non-porous polymer-based spheres (100058). The GACs, as provided by the manufacturers, are denoted as unfractionated fresh GACs in the following.

Grain size fractions of the 30N, K835 and Centaur with mean grain diameters of 0.30 mm (0.25 - 0.355 mm), 0.57 mm (0.50 - 0.63 mm) and 1.90 mm (1.80 - 2.00 mm) were prepared by sieving the unfractionated fresh GACs using a sieve tower (AS 200, Retsch, Germany) and, if necessary, by grinding the unfractionated fresh GACs using a ball mill (PM100, Retsch, Germany) prior to sieving. The 100058 GAC was used solely at the original monomodal grain size (d_p) provided by the manufacturer (0.55 mm). Before use, the fresh GACs were treated by: (i) soaking in ultrapure water for 24 h, (ii) evacuating the soaked GAC using a vacuum chamber until rising air bubbles could no longer be seen and (iii) washing and decantation of the GAC using ultrapure water until the supernatant was particle-free.

2.5 Physical characterisation of the GAC

Evaluation of the bed volume specific outer surface area a_o and the representative hydraulic grain size d_{hy} of the unfractionated GACs is described in Section A of the supplementary material (SM).

The internal surface area a_{BET}, the pore volume of micropores (<2 nm) and mesopores (2–50 nm), the pore size distribution (PSD) and the tortuosity of the fresh unfractionated GACs were determined from nitrogen adsorption/desorption isotherms (BELSORP-max, MicrotracBEL). The pore volume of macropores (>50 nm) was determined by mercury intrusion porosimetry (Pascal 140/440, Thermo Fisher Scientific). To further elucidate the morphology of the 100058 GAC, images were taken from a cross-section of a single GAC grain with a High Resolution Scanning Electron Microscope (FEI Nova NanoSEM, 5 kV). Further details on the experimental procedures of physical GAC characterisation are given in Section B of the SM.

2.6 Data analysis and calculation of bed-volume-based apparent first order rate constants

MCA is consumed in the GAC bed. According to equations (1) and (2) above it is expected to follow first-order kinetics with respect to MCA if reaction (1) was slower than reaction (2) and thus rate limiting. If reaction (2) was rate limiting, then second-order kinetics is expected. Finally, mass transport inside the pores may be rate-limiting (diffusion control). In that case a first-order reaction will remain first-order and a second-order reaction will turn into an apparent 1.5-order reaction. To take that into account, apparent rate constants for a pseudo first-order reaction were determined and the validity of that approach was verified in separate experiments (see Section 2.10).

For a fixed-bed reaction at stationary conditions, the apparent bed-volume-based reaction rate constant k_{app} is obtained according to:

$$k_{app} = \frac{1}{EBCT} \cdot \ln\left(\frac{c_{bed,in}}{c_{bed,out}}\right) \quad (3)$$

where $c_{bed,in}$ and $c_{bed,out}$ are the GAC bed's MCA in- and outflow concentrations and EBCT is the empty bed contact time, given by V_{bed}/Q_{bed}, where V_{bed} and Q_{bed} are the bed volume and the volumetric flow rate, respectively.

To ensure that all GAC in the filter bed was subjected to the almost same concentration of MCA, it was designed such that the change of the concentration from the inflow to the outflow of the bed was negligible. Generally, typical outflow concentrations of monochloramine over the course of an experiment were about 5% below the inflow concentration (see Figure 2).

Consequently, the measurement of the outflow concentration would have resulted in a lack of precision. To overcome that restriction, the outflow concentration was obtained from the decreasing mass of the MCA stock solution. The volumetric dosing rate (Q_{stock}) for any time t during an experiment is given by Equation 4:

$$Q_{stock}(t) = \frac{\left(\frac{dm_{stock}}{dt}\right)}{\rho_{stock}(T)} \quad (4)$$

Here, $\rho_{stock}(T)$ is the temperature-dependent density of the stock solution and m_{stock} is the recorded mass of the stock solution on the balance. The time-dependent mass loss dm_{stock}/dt was determined in time intervals of 0.5–1 h.

A mass balance for MCA around the tank of the FBR system yields:

$$Q_{bed} \cdot c_{bed,out}(t) - Q_{bed} \cdot c_{bed,in} + Q_{stock}(t) \cdot c_{stock} - Q_{stock}(t) \cdot c_{bed,in} + R_{sys}(t) = V_{sys} \cdot \left(\frac{dc_{bed,in}}{dt}\right) \quad (5)$$

220 Here R_{sys} accounts for a hypothetical loss of MCA in the system excluding the GAC
221 bed (e.g. through reaction at the glass or tube walls) and c_{stock} is the concentration of
222 the MCA stock solution. Preliminary experiments without GAC showed that MCA
223 removal in the FBR system without GAC was negligible, thus:

$$R_{sys} = 0 \quad (6)$$

224 Since $c_{bed,in}$ was kept constant, the capacity term in Equation 5 gives:

$$V_{sys}\left(\frac{dc_{bed,in}}{dt}\right) = 0 \quad (7)$$

225 Introducing Equations 6 and 7 into Equation 5 and rearranging yields:

$$c_{bed,out}(t) = \frac{Q_{stock}(t)}{Q_{bed}} \cdot \left(c_{bed,in} - c_{stock}\right) + c_{bed,in} \quad (8)$$

226 Introducing Equation 8 into Equation 3 gives the bed volume based rate constant k_{app}
227 at any time t.

228 **2.7 Catalyst surface-area-based rate constants**

229 As the reduction of MCA by GAC is a solid surface reaction, catalyst surface-area-
230 based apparent rate constants $k_{app,a}$ are calculated from the bed-volume-based rate
231 constants according to:

$$k_{app,a} = \frac{k_{app}}{a_0} \quad (9)$$

232 where a_0 is the bed-volume-specific outer surface area of the GAC in the FBR.

2.8 Conversion dependence of the overall reaction rate

Previous studies showed that the reactivity of GACs for MCA conversion decreased gradually over time (Scaramelli and Digiano, 1977). However, using the FBR system described above, the time needed to acquire the data for determination of the rate constant at a given time t was short compared to the time needed for a notable decrease of GAC reactivity. Thus, for each time t, the assumption of quasi-steady state was justified.

To describe the process of decreasing reactivity of the heterogeneous MCA–GAC reaction, conversion–time curves were determined in FBR experiments for all GACs until the reactivity was constant over time. The general shape of the conversion–time curves can indicate which one of the two widely recognised reaction models, the Progressive-Conversion Model (PCM) or the Shrinking-Core Model (SCM) (Levenspiel, 1999) is appropriate.

FBR experiments were conducted to determine k_{app} either at the beginning of the MCA–GAC reaction or after a certain time of operation, when stationary conditions were reached. The reactivity at the beginning of the reaction was determined after ~0.1 mmol g^{-1} of MCA per mass of GAC had been converted in the GAC bed. For these experiments, the fresh GACs were used as provided by the manufacturer.

To determine the reactivity under stationary conditions, the fixed-bed experiments were divided into two consecutive steps: (i) subjecting the GACs to monochloramine at $c_{bed,in}$ = 4.5 mg L^{-1} (as Cl_2), T = 30 °C and Q_{bed} = 40 L h^{-1} (equalling a superficial filter velocity of v_{bed} = 44.1 m h^{-1}) until no change in k_{app} was observed and stationary conditions were reached and, (ii) determination of k_{app} under various stationary operation conditions (e.g. different $c_{bed,in}$, T or v_{bed}). GACs operating under stationary

conditions were denoted as altered GACs. A detailed description of the FBR experiments is provided in the following sections. Table 1 summarises all experiments conducted.

Table 1: Operation conditions of the FBR experiments.

2.9 Temperature dependence of rate constants

The temperature dependence of k_{app} is described using the Arrhenius Equation:

$$k_{app}(T)=k_0 \cdot e^{-\frac{E_A}{R_0 T}} \quad (10)$$

Here, k_0 and E_A are the frequency factor and the activation energy, respectively. R_0 is the universal gas constant and T is the temperature. E_A is derived from the slope of the linear least-squares best fit of the correlation between $\ln(k_{app})$ and T^{-1} (Arrhenius plots) (Levenspiel, 1999).

To describe the temperature dependence of MCA conversion in the GAC filter, the activation energies E_A (see Equation 10) of the reaction for both the fresh and the altered unfractionated GACs: 30N, K835 and Centaur, were determined. In order to calculate E_A, k_{app} was experimentally determined in FBR experiments in a range of temperatures of 12 to 45 °C. Other process parameters except the temperature were kept constant (see Table 1).

2.10 Verification of first-order kinetics

To experimentally verify the first-order kinetic approach used in this study, the reactivity of the altered unfractionated K835 GAC was determined for various MCA inflow concentrations. The reproducibility of the measurement of k_{app} was determined from a set of four repeated experiments.

2.11 Impact of external mass transport on the overall reactivity

To assess the impact of pore diffusional mass transport on the overall reactivity of the GAC, the influence of extra-particle mass transport (film diffusion) on the overall reaction rate must be excluded (Ertl et al. 1997). To check for the absence of film diffusion resistance, $k_{app,a}$ was determined for different superficial flows (v_{bed}) for filter beds of the fresh and altered unfractionated K835 GAC. To guarantee comparable conditions in all experiments, the flow rate v_{bed} was adjusted to the actual catalyst volume (V_{bed}) such that the EBCT in the filter column was 2.88 s.

The mass transfer coefficient of MCA through the laminar film layer (k_f) was calculated according to Equation 11 (Worch, 2012).

$$k_f = \frac{Sh \cdot D_{bulk,MCA}}{d_{hy}} \quad (11)$$

Here Sh is the Sherwood number, which was calculated according to the empirical approaches of Williamson et al. (1963) and Gnielinski (1978), and $D_{bulk,MCA}$ is the bulk diffusion coefficient of MCA in water, which was calculated using the Wilke-Chang correlation with 2.03×10^{-5} cm^2 s^{-1} (at 30°C) (Wilke and Chang, 1955).

If the rate of mass transfer through the laminar film layer is much larger than the surface-based reaction rate constant, thus $k_f >> k_{app,a}$, external mass transfer limitation can be excluded.

2.12 Impact of internal mass transport on the overall reactivity

2.12.1 Impact of grain size

To check for the importance of grain size on the overall reactivity, k_{app} was determined for different grain size fractions of the altered 30N GAC. To further elucidate the impact of grain size, the Thiele modulus Φ was calculated according to Equation 12 (Levenspiel, 1999). The Thiele modulus is a dimensionless constant representing the ratio of the overall reaction rate to the diffusion rate of the reactant in the pore system.

$$\Phi = L \cdot \sqrt{\left(\frac{k_{app}}{\eta \cdot D_{E,MCA}} \right)} \tag{12}$$

Here, L is the diffusion path length within the adsorbent, which is $d_p/6$ assuming a spherical shape of the GAC grains (Levenspiel, 1999). $D_{E,MCA}$ is the effective diffusion coefficient of MCA in the pore system and η is the effectiveness factor. $D_{E,MCA}$ was determined based on the pore size distribution of the individual GACs using the random intersecting pore model (Harriott, 2003) and assuming surface diffusion of MCA in the pore system of the GACs to be negligible (Fairey and Speitel, 2007):

$$D_{E,MCA} = \frac{1}{\tau} \cdot \frac{\sum_{j=d_{MCA}}^{\infty} D_{bulk,\,MCA} \cdot \left(1 - \frac{d_{MCA}}{d_{p,j}}\right)^4 \cdot V_{p,j}}{\sum_{j=d_{MCA}}^{\infty} V_{p,j}} \tag{13}$$

Here, τ is the tortuosity factor of the GACs, $d_{p,j}$ and $V_{p,j}$ are the diameter and the incremental pore volume of a pore in the size fraction j as derived from the pore size distribution of the 30N GAC, and d_{MCA} is the minimal pore diameter of the GAC that is still accessible for a MCA molecule.

313 The effectiveness factor η is defined as the ratio of the reaction rate to the theoretical
314 reaction rate without diffusional limitations (Ertl et al., 1997). For a first-order reaction
315 taking place at a spherical grain, η could be determined as follows (Levenspiel, 1999):

$$\eta = \frac{1}{\Phi} \cdot \left(\frac{1}{\tanh 3\Phi} - \frac{1}{3\Phi} \right) \qquad (14)$$

316 Numerical solutions of Equations 12 and 14 give the corresponding values for Φ and
317 η.

2.12.2 Impact of pore size distribution

In this set of experiments, k_{app} was determined for the altered 30N, K835, Centaur and 100058 GACs. To exclude the influence of GAC grain size on k_{app} and to allow comparison between the GACs, filter beds of equal grain size fractions were used (0.50 mm (100058) and 0.57 mm (30N, K835, Centaur)) to study the effect of the pore size distribution. It will be discussed and proven in detail in Sections 3.6 and 3.7 below that the prerequisites for the comparison between carbons of different surface chemical properties are fulfilled.

3 Results and Discussion

3.1 Physical characterisation of the GACs

The physical characteristics of the GACs tested in this study are summarised in Table 2. More details and further discussion of the results are given in Section B of the SM. There, N_2 adsorption-desorption isotherms of the fresh unfractionated GACs and the corresponding pore size distributions (PSD) are shown in Figure B.1 and the grain size distribution of the fresh unfractionated GACs are shown in Figure B.2.

Table 2: Physical characterisation of the fresh unfractionated GACs 30N, K835, Centaur and 100058.

3.2 Verification of the first-order reaction kinetics

Figure 2 exemplarily shows time plots of $c_{bed,in}$ and $c_{bed,out}$ of one of the four repeated verification experiments, as well as k_{app}, as calculated according to Equation (3). Figure 2(A) shows the rapid decrease of the reaction rate constant until stationary conditions were reached after ~90 h. This is much shorter than the time reported in a previous study (1250–3000 h) (Fairey and Speitel, 2007), although comparable MCA inflow concentrations were used in both studies. This discrepancy can be attributed to the significant differences in EBCT of the respective GAC beds (30 s in Fairey and Speitel (2007) and 2.8 s in this work) and thus, the difference in the time needed to oxidise the GAC in the bed.

Figure 2(B) shows the determination of k_{app} at three different inflow concentrations that were adjusted after stationary conditions had been reached.

Figure 2: Reaction rate constant k_{app} for MCA removal at the K835 GAC at $c_{bed,in}$ of 4.5 mg L^{-1} (as Cl_2) until stationary conditions were reached (A) and at three additional inflow concentrations (9.0, 1.6 and 0.9 mg L^{-1} (as Cl_2)) (B). Error bars represent the standard deviation of k_{app} as determined by Gaussian error propagation (n = 50).

Figure 3 shows the linear least-squares regression analysis between k_{app} and $c_{bed,in}$. The slope of the linear regression was almost zero ($[0.4 \pm 0.21] \times 10^{-3}$ L mg^{-1} s^{-1}), which shows that the reaction rate constant was independent of the inflow concentration. This confirms the validity of the first-order approach used in Equation 3. This was also true for MCA concentrations that are as low as typically found in swimming pool water (e.g. 0–1.8 mg L^{-1} as Cl_2, (Weaver et al., 2009)). The repeatability standard deviation of k_{app} for the altered GAC K835 determined by four identical repeated validation experiments was ±0.006 s^{-1} (~±4%), which indicates a high reproducibility of the experimental method used.

Figure 3: Effect of MCA inflow concentration on the apparent reaction rate constant for MCA conversion at the altered unfractionated K835 GAC. The solid line represents the linear least-squares best fit and dashed lines represent the 95% confidence band of the regression. Errors bars represent the repeatability standard deviation (n = 63).

Additionally, to check for heterogeneity of the reaction, the Maitlis' test was conducted (Crabtree, 2012). In that, the loss of MCA in the tank of the FBR system was measured once during the course of an experiment while bypassing the GAC filter column.

371 Results confirmed that no MCA was degraded and thus, no reactive agents leached
372 from the GAC.

373 **3.3 Exclusion of extra-particle mass transfer limitations**

374 Figure 4 shows the dependence of the apparent surface-related reaction rate constant
375 $k_{app,a}$ (in m s^{-1}), determined experimentally, and of the theoretical mass transfer
376 coefficient of MCA in the laminar film layer k_f (in m s^{-1}), on the filter velocity v_{bed} for the
377 fresh and altered unfractionated GAC K835. It showed that $k_{app,a}$ was independent of
378 the superficial flow rate v_{bed} for both, the fresh and altered GAC ($p < 0.001$). As
379 mentioned above, two empirical approaches for the calculation of the Sherwood
380 number were used. It appeared that $k_{app,a}$ was ~4 times lower than k_f when the
381 Sherwood number was approximated according to Williamson et al. (1963) and
382 ~10 times lower when the approximation according to Gnielinski (1978) was used.
383 Similar results were obtained for the fresh 30N GAC (results not shown). This proves
384 that external mass transport is not limiting the overall reactivity (Worch, 2008) for MCA
385 removal in GAC filters over a wide range of superficial filter velocities for both fresh
386 and altered GACs.

387 In previous work it was assumed that the negligible impact of film diffusion on the
388 removal of dichloramine at GACs would also apply to the removal of MCA (Fairey and
389 Speitel, 2007; Kim and Snoeyink, 1980). Our results prove that this assumption is
390 justified.

Figure 4: Impact of filter velocity on the experimentally determined apparent surface-related reaction rate constant $k_{app,a}$ for MCA conversion and the theoretical mass transfer coefficient k_f of the unfractionated K835 GAC. Error bars represent the 95% confidence interval. Mass transfer coefficients k_f were calculated using a mean grain diameter $d_{hy,K835}$ of 1.39 mm. The dashed vertical line represents the recommended filter velocity for GAC filters in swimming pool water treatment in Germany (≤ 30 m h^{-1}) (DIN 19643-2, 2012).

3.4 Progress of the reaction until stationary conditions were reached

Figure 5(A) shows the conversion–time curves of MCA in the GAC filter for the 0.57 mm grain size fractions of the 30N, K835, Centaur and 100058 GAC. The respective reaction rates are given in Figures 5(B) and 5(C).

It is apparent that the conversion–time plot of MCA removal for the conventional GACs (30N, K835, Centaur), which comprise a homogeneously distributed and strongly microporous pore size distribution, is hyperbolic, while that of the 100058 GAC is sigmoid (S-shaped). The conversion–time behaviour is reflected in the behaviour of the reaction rate over time. k_{app} of the GACs 30N, K835 and Centaur drop continuously. Instead, k_{app} of the 100058 first shows an increase and then decreases continuously after a maximum has been reached after about 15 h.

The sigmoid conversion–time behaviour is often associated with a shift in the reaction-controlling mechanism from chemical reaction rate control to diffusional control and can be described by the Shrinking-Core Model (SCM) (Levenspiel, 1999). The SCM describes a reaction that starts first at the outer surface of the GAC grains, and the reaction front then moves towards the centre of the grains with ongoing reaction time

(Levenspiel, 1999). The difference in conversion–time behaviour between the microporous GACs and the 100058 GAC is explained in more detail in Section C of the SM.

Figure 5: MCA removed (A) and bed volume-based reaction rate constant k_{app} for MCA removal (B, C) over the filter run time. All GACs had the same grain size of ~0.55 mm (0.57 mm for the 100058 GAC). Dashed horizontal lines in (B) represent the GAC reactivity when stationary conditions were reached.

3.5 Impact of grain size

Figure 6(A) presents the time course of the bed-volume based first-order reaction rate constant k_{app} for MCA removal by different grain size fractions of the 30N GAC until stationary conditions were reached. The bed-volume-based reaction rate constants at stationary conditions are displayed in 6(B). They decrease linearly with increasing grain diameter. These results are in agreement with previous studies which, however, were obtained before stationary conditions were reached (Komorita and Snoeyink, 1985).

Figure 6: (A) Reaction rate constant k_{app} over the filter runtime for different grain size fractions of the 30N GAC. Dashed horizontal lines represent the level of GAC reactivity at stationary conditions. (B) k_{app} and (C) $k_{app,a}$ at stationary conditions as function of the grain diameter. Open circle symbols in (B) and (C) represent k_{app} for the unfractionated 30N GAC using $d_{hy,30N}$ = 1.18 mm as representative grain size (data not shown in A). Error bars in (B) and (C) represent the 95% confidence intervals.

Figure 6(C) shows the catalyst surface-area-related rate constants for different grain size fractions of the 30N carbon. If the reaction only took place at the outer surface of the GAC grains, then $k_{app,a}$ would be independent of the grain diameter. The decrease indicates that diffusional resistances in the pore systems are limiting the overall reaction rate.

To assess further the influence of pore diffusion on the overall reactivity, the Thiele modulus Φ and the effectiveness factor η were calculated using the stationary effective bed-volume-based reaction rate constants. The minimal pore diameter of the GAC that is accessible for the MCA molecule, d_{MCA}, was needed in equation (13). As will be discussed further in Section 3.6, d_{MCA} was assumed to be approximately twice the molecular diameter of the MCA molecule. The individual tortuosity factors τ of the carbons needed to determine d_{MCA} were calculated using the CSTM model and are given in Section B of the SM.

Figure 7 shows Φ as function of η. The Thiele modulus of the grain size fractions 1.9 mm, 1.18 mm (unfractionated GAC) and 0.57 mm were >4, which confirmed that pore diffusion strongly controls the overall reaction. The Thiele modulus of the smallest grain size fraction (0.30 mm) was 3, which is related to the transient region with moderate pore diffusional influence (Levenspiel, 1999). In a previous study (Scaramelli and Digiano, 1977) a Thiele modulus of 0.51 was found for a GAC with a grain size of ~0.5 mm. The Thiele modulus of the 0.57 mm fraction of the 30N GAC observed in this study was higher by a factor of ~15. This indicates that the importance of pore diffusion on the overall reactivity found in this study was higher compared to the previous results. This discrepancy is due to the fact that $D_{E,MCA}$ of the 30N GAC (9.43×10^{-7} $cm^2\ s^{-1}$) used to calculate Φ in the present study was lower by a factor of ~4 compared to that used previously, where an estimated $D_{E,MCA}$ of 5.484×10^{-6} $cm^2\ s^{-1}$ was used (Scaramelli and Digiano, 1977). However, they had no data available regarding the pore size distribution and based their estimation on the GACs porosity and roughly estimated tortuosity.

Figure 7: Effectiveness factor η of the MCA-GAC reaction at stationary conditions for different grain size fractions of the 30N GAC as function of the Thiele modulus Φ. Open triangle symbols represent k_{app} for the unfractionated 30N GAC using $d_{hy,30N}$ = 1.18 mm. Filled triangle symbols represent k_{app} for the fractionated 30N GAC. The dashed black line is for orientation only and represents the expected relationship between Φ and η as discussed elsewhere (Ertl et al., 1997). Error bars represent the 95% confidence intervals

3.6 Impact of pore size distribution

The magnitudes of Φ and η (Figure 7) demonstrate a very strong limitation of the overall reaction rate by diffusion. Consequently, it is concluded that k_{app} is not, or only to a minor extent, affected by the intrinsic chemical reaction, which most likely differs among the different types of carbons tested.

Given the strong pore diffusional control of the overall reaction, conclusively, values of k_{app} for the given set of equally sized GACs (Figure 5) are primarily affected by the effective diffusion coefficient of MCA in the pore system ($D_{E,MCA}$), which in turn is a function of the pore size distribution (Equation 13). Thus, the GAC that exhibits the highest $D_{E,MCA}$ should exhibit the highest k_{app} and vice versa.

Using the effective molecular diameter of MCA of ~0.5 nm (calculated using the RasMol visualisation tool (Sayle and Milnerwhite, 1995)) as d_{MCA} in Equation 13 to calculate $D_{E,MCA}$ for the different GACs) gives the following order of $D_{E,MCA}$: 2.28×10^{-6} cm² s^{-1} (30N) > 1.42×10^{-6} cm² s^{-1} (K835) > 1.26×10^{-6} cm²s^{-1} (Centaur). Obviously, this order does not comply with the order of k_{app} shown in Figure 8 (0.036 s^{-1} (Centaur) > 0.025 s^{-1} (K835) > 0.017 s^{-1} (30N) > 0.016 s^{-1} (100058)).

By calculating $D_{E,MCA}$ as a function of d_{MCA}, it appeared that the orders of $D_{E,MCA}$ and k_{app} correspond when d_{MCA} is equal or larger than ~1.3 nm. This leads to the conclusion that pores <1.3 nm in width, which is about 2.5 times the molecular diameter of a MCA molecule, might be barely accessible for MCA. This can be explained by constrictions at the pore mouth caused by water molecules that adsorb onto oxygen-containing functional groups present at the GAC surface by hydrogen bonding (McCallum et al., 1999). These findings are in agreement with those found in previous studies, where it

was assumed that certain pores might be barely accessible for MCA molecules due to diffusional limitations (Fairey et al., 2006).

The significantly higher $D_{E,MCA}$ found for the Centaur GAC for d_{MCA} >1.3 nm compared to the 30N and K835 GAC results mainly from the large number of mesopores (>7 nm), which the other GACs did not contain. It must be noted here that calculation of $D_{E,MCA}$ for the 100058 GAC according to Equation 13 is not eligible due to the structured pore size distribution of the GAC grains (Harriott, 2003).

3.7 Impact of water temperature

Figure 8 presents Arrhenius plots for MCA removal in GAC beds of the 30N, K835 and Centaur GAC, determined at temperatures between 12 and 45 °C. The activation energies E_A of the fresh and altered GACs derived from the Arrhenius plots ranged between 20.4 and 29.8 kJ mol^{-1}. For typical swimming pool water temperatures (20 to 35 °C) an increase of activation energy from 20 to 30 kJ mol^{-1} results in an increase in the reaction rates of 40% (fresh GACs) and 80% (altered GACs).

For the fresh unfractionated GACs investigated (30N and K835), activation energies were between 20.4 and 21.4 kJ mol^{-1}. For the altered unfractionated GACs investigated (30N, K835 and Centaur) they were slightly higher, namely between 26.0 and 29.3 kJ mol^{-1}. However, the differences were not significant ($p < 0.001$).

The activation energies determined are those for the combined pore diffusion – surface reaction process. It is interesting to note that temperature sensitivity was higher when the GACs had been altered, i.e. for lower overall reaction rates. For most chemical reactions, the activation energy is in the range of 50 to 250 kJ mol^{-1}. For diffusional mass transport in water, the diffusion coefficient is approximately linearly proportional

527 to T. From that, an activation energy for diffusion in water of approximately 5 kJ mol^{-1}
528 can be calculated

529 For the temperature dependence of the combined processes of diffusion and chemical
530 surface reaction in pores, it will consequently be lower for diffusion-controlled
531 processes, i.e. when the chemical surface reaction is faster, and will be higher for
532 chemical surface reaction-controlled processes. Thus, as the alteration of the GACs
533 brings about a decrease in a chemical reaction rate, the higher activation energies
534 found for the altered GACs (although not significant due to the small number of data
535 points available) support the conclusions on diffusion control drawn above, as diffusion
536 limits less for slower chemical reactions.

537 Additionally, the conclusions on diffusion control are supported by the fact that
538 activation energies found for MCA removal in GAC filters in this study were significantly
539 lower than those reported for the removal of dichloramine (35.6 kJ mol^{-1} at pH 10 (Kim
540 and Snoeyink, 1978)) and free chlorine (43.9 kJ mol^{-1} at pH 7.6 (Suidan and Snoeyink,
541 1977)). The lower activation energies are in agreement with the higher reactivity of
542 GACs for the removal of dichloramine and free chlorine as compared with MCA.

543 As shown previously in this study, the impact of pore diffusion increases with increasing
544 grain size of the GACs used. Consequently, this increase in diffusional resistance
545 should affect the temperature dependence of the overall reaction as well (Levenspiel,
546 1999). However, the difference in the experimentally determined E_A for the
547 unfractionated 30 N carbon (1.18 mm grain diameter) and the 0.5 mm size fraction of
548 the 30N GAC was not significant ($p < 0.001$). This discrepancy can be explained by the
549 limited resolution of the method used to determine k_{app}, which in turn is used to
550 calculate E_A.

Figure 8: Impact of water temperature on the apparent reaction rate constant for MCA conversion at the GACs 30N, K835 and Centaur. Solid lines represent linear least-squares best fit and dashed lines represent the 95% confidence band of the fitted regression. Errors for E_A represent the standard deviation of the slope of the linear regression (n = 2 – 6, depending on the carbon). (n.d. = not determined)

4 Summary and conclusions

Using a fixed bed reactor system, the thorough investigation of apparent reaction rates of the removal of monochloramine at GAC surfaces showed a rapid decrease with ongoing exposure of the GAC to monochloramine. Quasi-stationary conditions were reached after less than 100 h, when the GAC had been exposed to MCA concentrations of 4.5 mg L^{-1}.

When quasi-stationary conditions had been reached, film diffusion definitely is not rate-limiting. However, diffusion of monochloramine in the pores, for the GACs investigated, limits the overall reaction rate. It was shown that the overall apparent reaction including diffusion and chemical reaction is first-order. As diffusion limitation of a second-order chemical reaction will result in an apparent 1.5-order overall reaction, and diffusion limitation of a first-order reaction will result in an apparent first-order overall reaction rate, it is concluded that the reaction according to equation (2) is much faster than the reaction according to equation (1) or not taking place at all.

The dependence of the apparent overall reaction rate on temperature yielded activation energies E_A, according to the Arrhenius relation, in the range of 20 – 27 kJ mol^{-1}. This additionally supports the conclusion that diffusion is ratee-limiting as chemical reactions usually show activation energies of 50 kJ mol^{-1} or higher, while temperature dependence of diffusion is equivalent to activation energies of about 10 kJ mol^{-1}.

Also, the Thiele modulus (3.0 – 42.1), derived from experiments with different grain sizes, indicates that the overall reaction rate is strongly controlled by diffusional mass transport in the pore system of the GACs considered. Conclusively, the pore size

582 distribution of the GACs was found to have a significant impact on the overall reaction
583 rate constant of MCA removal in GAC filters.

584 Analysis of the impact of the pore size distribution indicates that pores <1.3 nm, which
585 is about 2.5 times the molecular diameter of MCA, are not accessible for the MCA–
586 GAC reaction. Instead, the number of large mesopores is suggested to be of
587 importance for a high overall reactivity of a GAC bed for MCA removal.

588 The use of smaller grain size fractions resulted in an increase of the overall reactivity
589 of the GAC bed, which is attributed to a lower diffusion path length in the single GAC
590 grains. If for example swimming pool water with a MCA concentration of 0.2 mg L^{-1} is
591 treated in a GAC bed of 1 m height of the 30N GAC and of the largest grain size
592 investigated (1.9 mm), the effluent concentration will be 0.038 mg L^{-1}. For the smallest
593 grain size (0.3 mm) this effluent concentration can be achieved with a GAC bed of 0.56
594 m.

595 However, it must be considered that the use of smaller GAC grain sizes for enhanced
596 MCA removal in full-scale applications would bring about a considerably high pressure
597 loss in fixed-bed GAC filters. For the example described above, using the empirical
598 relationship described by Ergun (Ergun, 1952) and 1 m bed of 1.9 mm grains, the
599 pressure loss will be 1.6 mbar. However, for a 0.56 m bed of the 0.3 mm grains, the
600 pressure loss will 24 mbar, i.e. higher by a factor of 15.

601

602 From the shape of the conversion–time curves of the reaction it was concluded that
603 the decrease of the reactivity of the GACs observed in the initial phase of the MCA–
604 GAC reaction is due to an increasing pore diffusional resistance that developed with

increasing reaction time. The increasing diffusional control is explained by the fact that the reaction front starts at the outer surface of the grains and then moves towards the centre of the GAC grains.

Acknowledgements

Dr. Constantinos Salmas is thanked for simulations with the CSTM model. Dr. Irena Senkovska and Dr. Stephan Böttcher are appreciated for performing the N_2 physisorption and mercury intrusion measurement and for giving advice for QSDFT analysis. Stefan Rößler and Duo Xu are thanked for their preliminary work in developing the experimental setup. Jana Brückner, Gerit Orzechowski and Pascal Müller are acknowledged for their considerable continuous support in the laboratory. Dr. Viktor Schmalz and Illyea Hawke are thanked for their valuable input and the proof reading of the manuscript. Mention of trade names, commercial products or services does not constitute endorsement or recommendation of use.

Abbreviations

EBCT	Empty bed contact time
FBR	Fixed-bed reactor
GAC	Granular activated carbon
MCA	Monochloramine
NDMA	N-Nitrosodimethylamine
PCM	Progressive Conversion Model
PSD	Pore size distribution
QSDFT	Quenched solid density functional theory
SCM	Shrinking-Core Model
SEM	Scanning Electron Microscopy

Symbols

a_o	bed volume specific outer surface area ($m^2\ m^{-3}$)
$c_{bed,in}$	MCA in-flow concentrations of a GAC filter (mg L^{-1} as Cl_2)
$c_{bed,out}$	MCA out-flow concentrations of a GAC filter (mg L^{-1} as Cl_2)
c_{stock}	Concentration of the MCA stock solution (mg L^{-1} as Cl_2)
$D_{bulk,MCA}$	Bulk diffusion coefficient of MCA in water ($m^2\ s^{-1}$)
$D_{E,MCA}$	Effective diffusion coefficient of MCA in the pore system of a GAC grain ($m^2\ s^{-1}$)
d_{hy}	Hydraulic diameter (m)

d_{MCA}	Minimum pore diameter of a GAC that is still accessible for an MCA molecule (nm)
$d_{p,i}$	Pore diameter of pore size i (nm)
E_A	Activation energy (J mol^{-1})
k_{app}	Observable pseudo-first-order reaction rate constant (s^{-1})
$k_{app,a}$	Pseudo-first-order reaction rate constant normalised by the specific outer surface a_o of the GAC in the filter bed (m s^{-1})
k_0	Frequency factor (s^{-1})
k_f	Mass transfer coefficient of MCA through the laminar film layer (m s^{-1})
L	Diffusion path length within the adsorbent (m)
pH	pH value
Q	Volumetric fluid flow rate (L s^{-1})
Q_{bed}	Volumetric fluid flow through a GAC bed (L s^{-1})
Q_{stock}	Volumetric dosing rate of an MCA stock solution (L s^{-1})
R_0	Universal gas constant (R = 8.314 J K^{-1} mol^{-1})
R_{sys}	Time-dependent loss of MCA in the system without GAC filter (mg s^{-1} as Cl_2)
Sh	Sherwood number (dimensionless)
T	Temperature (K)
t_{EBCT}	Empty bed contact time (EBCT) (s)
V_{bed}	Bed volume (L)
v_{bed}	Superficial filter velocity (m s^{-1})

V_{sys}	Water volume in the FBR system (L)
z_{bed}	Bed depth (m)

Greek symbols

ε	Molar absorption coefficient (mol^{-1} cm^{-1})
η	Effectiveness factor of a heterogeneous reaction (dimensionless)
$\rho_{stock}(T)$	Temperature-dependent density of an MCA stock solution ($g\ L^{-1}$)
τ	Tortuosity factor of a GAC (dimensionless)
Φ	Thiele modulus of a heterogeneous reaction (dimensionless)

References

Aleghafouri, A., Mohsen-Nia, M., Mohajeri, A., Mahdyarfar, M., Asghari, M., 2012. Micropore size analysis of activated carbons using nitrogen, carbon dioxide and methane adsorption isotherms: Experimental and theoretical studies. Adsorption Science and Technology 30, 307-316.

ANSI/APSP-1, 2009. American National Standard for Water Quality in Public Pools and Spas. The Association of Pool and Spa Professionals. Alexandria.

Aoki, T., 1989. Continuous-Flow Method for Simultaneous Determination of Monochloramine, Dichloramine, and Free Chlorine - Application to a Water-Purification Plant. Environmental Science and Technology 23, 46-50.

Bashkova, S., Baker, F.S., Wu, X.X., Armstrong, T.R., Schwartz, V., 2007. Activated carbon catalyst for selective oxidation of hydrogen sulphide: On the influence of pore structure, surface characteristics, and catalytically-active nitrogen. Carbon, 45, 1354-1363.

Bauer, R.C., Snoeyink, V.L., 1973. Reactions of Chloramines with Active Carbon. Journal of the Water Pollution Control Federation 45, 2290-2301.

Bernard, A., Carbonnelle, S., Michel, O., Higuet, S., de Burbure, C., Buchet, J.P., Hermans C., Dumont, X., Doyle, I., 2003. Lung hyperpermeability and asthma prevalence in schoolchildren: Unexpected associations with the attendance at indoor chlorinated swimming pools. Occupational and Environmental Medicine 60, 385-394.

Bernard, A., Nickmilder, M., Voisin, C., 2008. Outdoor swimming pools and the risks of asthma and allergies during adolescence. European Respiratory Journal 32, 979-988.

Blatchley, E.R., Cheng, M.M., 2010. Reaction Mechanism for Chlorination of Urea. Environmental Science and Technology 44, 8529-8534.

Consolazio, C.F., Johnson, R.E., Pecora, L.J., 1963. Physiological Measurements of Metabolic Functions in Man. McGraw-Hill, New York.

Crabtree, R.H., 2012. Resolving Heterogeneity Problems and Impurity Artifacts in Operationally Homogeneous Transition Metal Catalysts. Chemical Reviews 112, 1536-1554.

Deborde, M., von Gunten, U., 2008. Reactions of chlorine with inorganic and organic compounds during water treatment - Kinetics and mechanisms: A critical review. Water Research 42, 13-51.

DIN 19643-2, 2012. Treatment of water of swimming pools and baths, Part 2: Combinations of process with fixed bed filters and precoat filters (in German: Aufbereitung von Schwimm- und Badebeckenwasser, Teil 2: Verfahrenskombinationen mit Festbett- und Anschwemmfiltern). Normenausschuss Wasserwesen (NAW) im DIN Deutsches Institut für Normung. Beuth Verlag, Berlin.

DIN EN ISO 7393-2, 2000. Water quality - Determination of free chlorine and total chlorine, Part 2: Colorimetric method using N,N-diethyl-1,4-phenylenediamine, for routine control purposes (in German: Wasserbeschaffenheit - Bestimmung von freiem Chlor und Gesamtchlor, Teil 2: Kolorimetrisches Verfahren mit

717 N,N-Diethyl-1,4-Phenylendiamin für Routinekontrollen). Normenausschuss
718 Wasserwesen (NAW) im DIN Deutsches Institut für Normung. Beuth Verlag,
719 Berlin.

720 Eichelsdörfer, D., Slovak, D., Dirnagl, D., Schmidt, K., 1975. Zur Reizwirkung
721 (Konjuctivitis) von Chlor und Chloraminen im Schwimmbeckenwasser (in
722 German). Vom Wasser 45, 17-28.

723 Ergun S., 1952. Fluid Flow through Packed Columns. Chemical Engineering Progress
724 48, 89-94.

725 Ertl, G., Knözinger, H., Weitkamp, J., 1997. Handbook of heterogeneous catalysis.
726 VCH Verlagsgesellschaft mbH, Weinheim.

727 Fairey, J.L., Speitel, G.E., Katz, L.E., 2006. Impact of natural organic matter on
728 monochloramine reduction by granular activated carbon: The role of porosity and
729 electrostatic surface properties. Environmental Science and Technology 40,
730 4268-4273.

731 Fairey, J.L., Speitel, G.E., Katz, L.E., 2007. Monochloramine destruction by GAC -
732 Effect of activated carbon type and source water characteristics. Journal of the
733 American Water Works Association 99, 110-120.

734 Gnielinski, V., 1978. Gleichungen zur Berechnung des Wärme- und Stoffaustausches
735 in durchströmten ruhenden Kugelschüttungen bei mittleren und großen
736 Pecletzahlen (in German). Verfahrenstechnik 12, 363-366.

737 Hand, V.C., Margerum, D.W., 1983. Kinetics and Mechanisms of the Decomposition
738 of Dichloramine in Aqueous-Solution. Inorganic Chemistry 22, 1449-1456.

739 Harriott, P., 2003. Chemical reactor design. Marcel Dekker, New York.

740 Jaguaribe, E.F., Medeiros, L.L., Barreto, M.C.S., Araujo, L.P., 2005. The performance
741 of activated carbons from sugarcane bagasse, babassu, and coconut shells in
742 removing residual chlorine. Brazilian Journal of Chemical Engineering 22, 41-47.

743 Kim, B.R., 1977. Analysis of batch and packed bed reactor models for the carbon-
744 chloramine reactions. Doctoral thesis. University of Illinois at Urbana-Champaign,
745 Illinois.

746 Kim, B.R., Snoeyink, V.L., Schmitz, R.A., 1978. Removal of dichloramine and ammonia
747 by granular carbon. Journal of the Water Pollution Control Federation 50, 122-
748 133.

749 Kim, B.R., Snoeyink, V.L., 1980. The Monochloramine-GAC Reaction in Adsorption
750 Systems. Journal of the American Water Works Association 72, 488-490.

751 Komorita, J.D., Snoeyink, V.L., 1985. Monochloramine Removal from Water by
752 Activated Carbon. Journal of the American Water Works Association 77, 60-60.

753 Levenspiel, O., 1999. Chemical reaction engineering, Third Edition. John Wiley &
754 Sons, New York.

755 Mangun, C.L., Braatz, R.D., Economy, J., Hall, A.J., 1999. Fixed bed adsorption of
756 acetone and ammonia onto oxidized activated carbon fibers. Industrial and
757 Engineering Chemistry Research 38, 3499-3504.

758 Maia, F., Silva, R., Jarrais, B., Silva, A.R., Freire, C., Pereira, M.F.R., Figueiredo, J.L.,
759 2008. Pore tuned activated carbons as supports for an enantioselective
760 molecular catalyst. Journal of Colloid and Interface Science 328, 314-323.

761 McCallum, C.L., Bandosz, T.J., McGrother, S.C., Muller, E.A., Gubbins, K.E., 1999. A
762 molecular model for adsorption of water on activated carbon: Comparison of
763 simulation and experiment. Langmuir 15, 533-544.

764 Qiang, Z.M., Adams, C.D., 2004. Determination of monochloramine formation rate
765 constants with stopped-flow spectrophotometry. Environmental Science and
766 Technology 38, 1435-1444.

767 Radian, A., Carmeli, M., Zadaka-Amir, D., Nir, S., Wakshal, E., Mishael, Y.G., 2011.
768 Enhanced removal of humic acid from water by micelle-montmorillonite
769 composites: Comparison to granulated activated carbon. Applied Clay Science
770 54, 258–263.

771 Sayle, R.A., Milnerwhite, E.J., 1995. Rasmol - Biomolecular Graphics for All. Trends in
772 Biochemical Sciences 20, 374-376.

773 Scaramelli, A.B., Digiano, F.A., 1977. Effect of sorbed organics on efficiency of
774 ammonia removal by chloramine-carbon surface-reactions. Journal of the Water
775 Pollution Control Federation 49, 693-705.

776 Schreiber, B., Brinkmann, T., Schmalz, V., Worch, E., 2005. Adsorption of dissolved
777 organic matter onto activated carbon - the influence of temperature, absorption
778 wavelength, and molecular size. Water Research 39, 3449-3456.

779 Schreiber, I.M., Mitch, W.A., 2005. Influence of the order of reagent addition on NDMA
780 formation during chloramination. Environmental Science and Technology 39,
781 3811-3818.

782 Schreiber, I.M., Mitch, W.A., 2006. Nitrosamine formation pathway revisited: The
783 importance of chloramine speciation and dissolved oxygen. Environmental
784 Science and Technology 40, 6007-6014.

785 Schurter, L.M., Bachelor, P.P., Margerum, D.W., 1995. Nonmetal Redox Kinetics -
786 Monochloramine, Dichloramine, and Trichloramine Reactions with Cyanide Ion.
787 Environmental Science and Technology 29, 1127-1134.

788 Sparks, D.L., 1989. Kinetics of Soil Chemical Processes. Academic Press, New York.

789 Suidan, M.T., Snoeyink, V.L., Schmitz, R.A., 1977. Reduction of Aqueous Free
790 Chlorine with Granular Activated Carbon, pH and Temperature Effects.
791 Environmental Science and Technology 11, 785-789.

792 Walse, S.S., Mitch, W.A., 2008. Nitrosamine carcinogens also swim in chlorinated
793 pools. Environmental Science and Technology 42, 1032-1037.

794 Weaver, W.A., Li, J., Wen, Y.L., Johnston, J., Blatchley, M.R., Blatchley, E.R., 2009.
795 Volatile disinfection by-product analysis from chlorinated indoor swimming pools.
796 Water Research 43, 3308-3318.

797 Williamson, J.E., Bazaire, K.E., Geankoplis, C.J., 1963. Liquid-Phase Mass Transfer
798 at Low Reynolds Numbers. Industrial and Engineering Chemistry Fundamentals
799 2, 126-129.

800 Wilke, C.R., P. Chang, 1955. Correlation of Diffusion Coefficients in Dilute Solutions.
801 American Institute of Chemical Engineers Journal 1 264-270.

802 Worch, E., 2008. Fixed-bed adsorption in drinking water treatment: a critical review on
803 models and parameter estimation. Journal of Water Supply Research and
804 Technology-Aqua 57, 171-183.

805 Worch, E., 2012. Adsorption Technology in Water Treatment: Fundamentals,
806 Processes, and Modeling. Walter de Gruyter GmbH & Co. KG, Berlin/Boston.

807 Zwiener, C., Richardson, S.D., De Marini, D.M., Grummt, T., Glauner, T., Frimmel,
808 F.H., 2007. Drowning in disinfection byproducts? Assessing swimming pool
809 water. Environmental Science and Technology 41, 363-372.

810

811 **Tables**

812

813 Table 1: Operation conditions of the FBR experiments.

Type of study	GACs	Parameters varied	Parameters kept constant
Verification of the kinetic first-order approach	K835 *(unfractionated)*	$c_{bed,\ in}$ = 0.5 - 9 mg L^{-1} (as Cl_2)	v_{bed} = 44.1 m h^{-1} T = 30 °C V_{bed} = 32 mL h_{bed} = 3.5 cm t_{EBCT} = 2.88 s
Extra-particle mass transfer	K835, 30N *(unfractionated)*	v_{bed} = 8.3 - 132.2 m h^{-1} V_{bed} = 6 - 96 mL h_{bed} = 0.6 - 94 cm	T = 30 °C $c_{bed,\ in}$ = 4.5 mg L^{-1} (as Cl_2) t_{EBCT} = 2.88 s
Impact of grain size	30N *(size fractions and unfractionated)*	d_{grain} = 0.30 - 1.9 mm	v_{bed} = 44.1 m h^{-1} T = 30 °C $c_{bed,\ in}$ = 4.5 mg L^{-1} (as Cl_2) V_{bed} = 32 mL h_{bed} = 3.5 cm t_{EBCT} = 2.88 s
Temperature dependence	30N, K835, Centaur *(unfractionated)*	T = 12 - 45 °C	v_{bed} = 44.1 m h^{-1} $c_{bed,\ in}$ = 4.5 mg L^{-1} (as Cl_2) V_{bed} = 32 mL h_{bed} = 3.5 cm t_{EBCT} = 2.88 s
Conversion dependence and impact of pore size distribution	30N, K835, Centaur and 100058 *(0.57 mm size fraction)*	-	v_{bed} = 44.1 m h^{-1} T = 30 °C $c_{bed,\ in}$ = 4.5 mg L^{-1} (as Cl_2) V_{bed} = 32 mL h_{bed} = 3.5 cm t_{EBCT} = 2.88 s

814

815

816

817 Table 2: Physical characterisation of the fresh unfractionated GACs 30N, K835, Centaur and 100058.

GAC type	Hydraulic diameter d_{hy}, in mm	Outer surface a_o in $m^2\ m^{-3}$ [a]	Inner surface a_{BET} in $m^2\ g^{-1}$ [a,b]	Specific pore volume in $cm^3\ g^{-1}$ (%)				
				Total	Micropores	Mesopores (total)	Mesopores >7 nm [d]	Macro-pores
30N	1.18	5444	1105 (900 [e])	0.522	0.411 (79)	0.092 (18)	0.003 (0.6)	0.019 (4)
K835	1.39	4480	1073 (1170 [f])	0.446	0.419 (94)	0.020 (5)	0.001 (0.2)	0.007 (2)
Centaur	1.00	5532	895 (815 [g])	0.408	0.353 (87)	0.046 (11)	0.015 (3.7)	0.009 (2)
100058	0.55	17418	1291 (1350 [c])	0.605	0.496 (82)	0.102 (17)	0.013 (2.1)	0.007 (1)

818 [a]… All pores of the activated GACs were potentially accessible for the MCA conversion reaction (differences in BET surfaces between granular GACs and their powdered
819 counterparts were <5%).
820 [b] … Values in brackets represent data as found in the literature.
821 [c] … As reported by the manufacturer.
822 [d] … As derived from the PSD.
823 [e] … Radian et al., 2011.
824 [f] … Aleghafouri et al., 2012.
825 [g] … Bashkova et al., 2007.
826

827 **Figures**

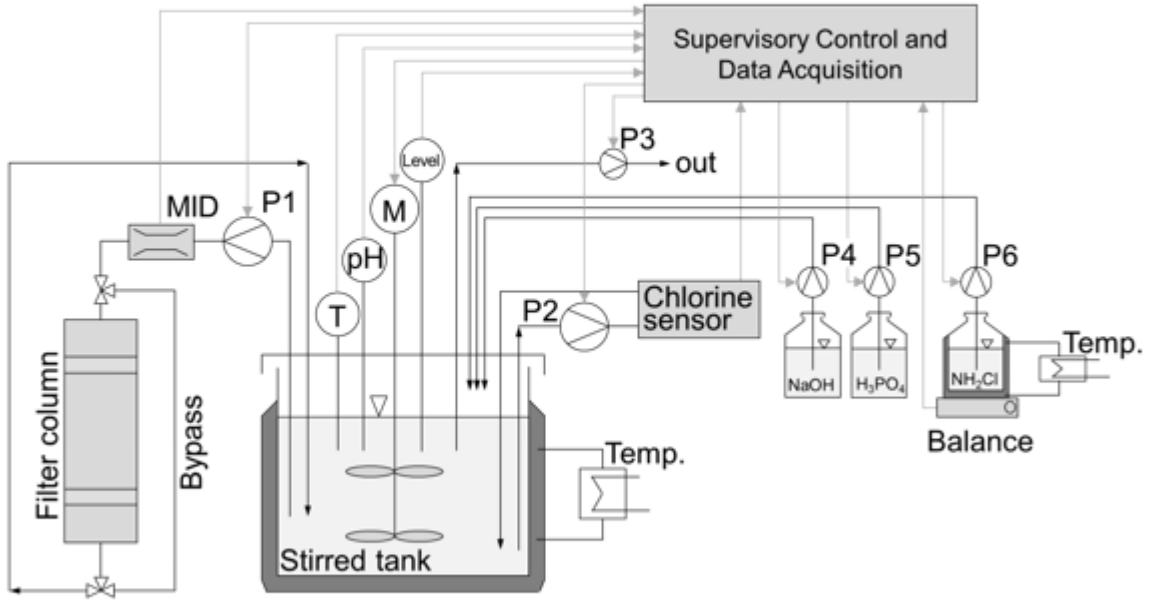

828

829 Figure 1: Scheme of the laboratory-scale FBR system.

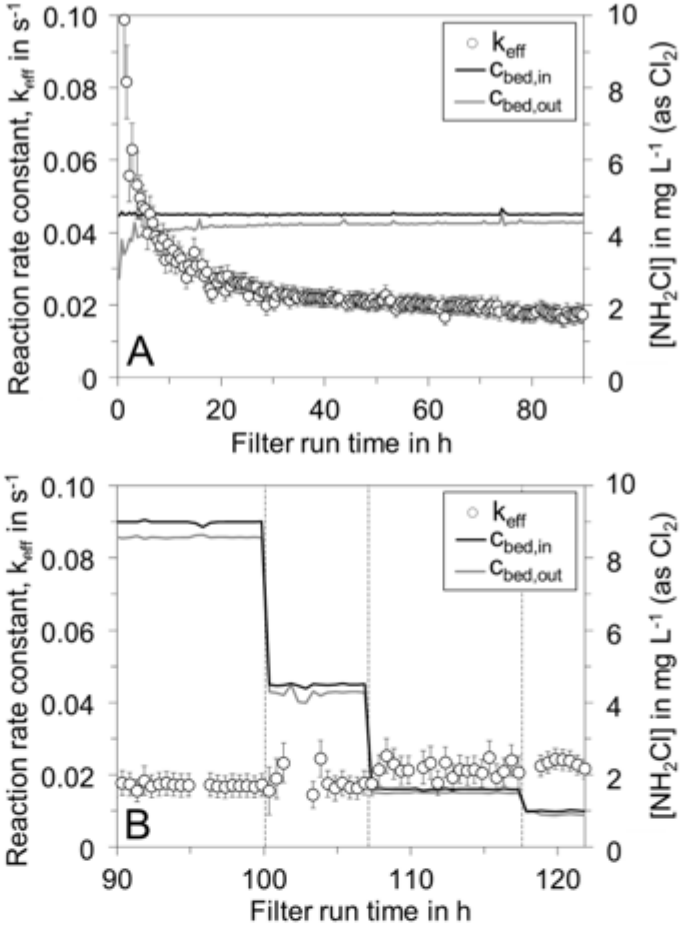

Figure 2: Reaction rate constant k_{app} for MCA removal at the K835 GAC at $c_{bed,in}$ of 4.5 mg L^{-1} (as Cl_2) until stationary conditions were reached (A) and at three different inflow concentrations (9.0, 4.5, 1.6 and 0.9 mg L^{-1} (as Cl_2)) (B). Error bars represent the standard deviation of k_{app} as determined by Gaussian error propagation (n = 50).

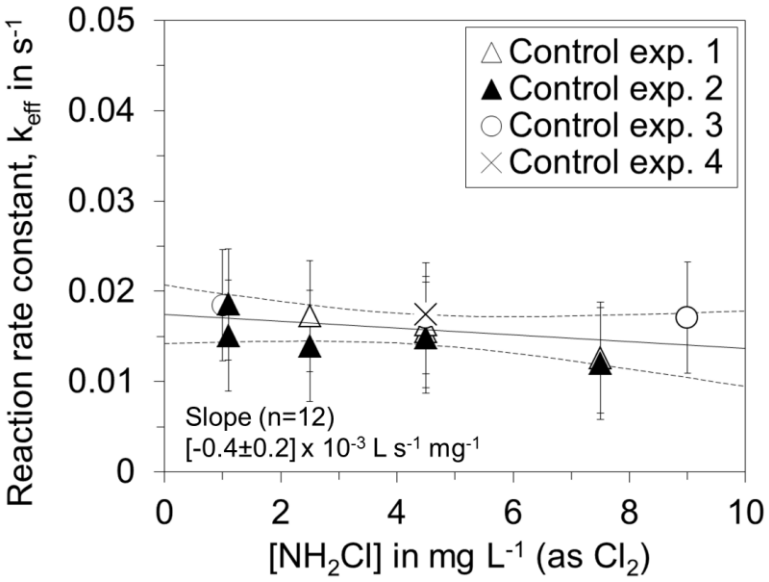

836

837 Figure 3: Effect of MCA inflow concentration on the apparent reaction rate

838 constant for MCA conversion at the altered unfractionated K835

839 GAC. The solid line represents the linear least-squares best fit and

840 dashed lines represent the 95% confidence band of the regression.

841 Errors bars represent the repeatability standard deviation (n = 63).

842

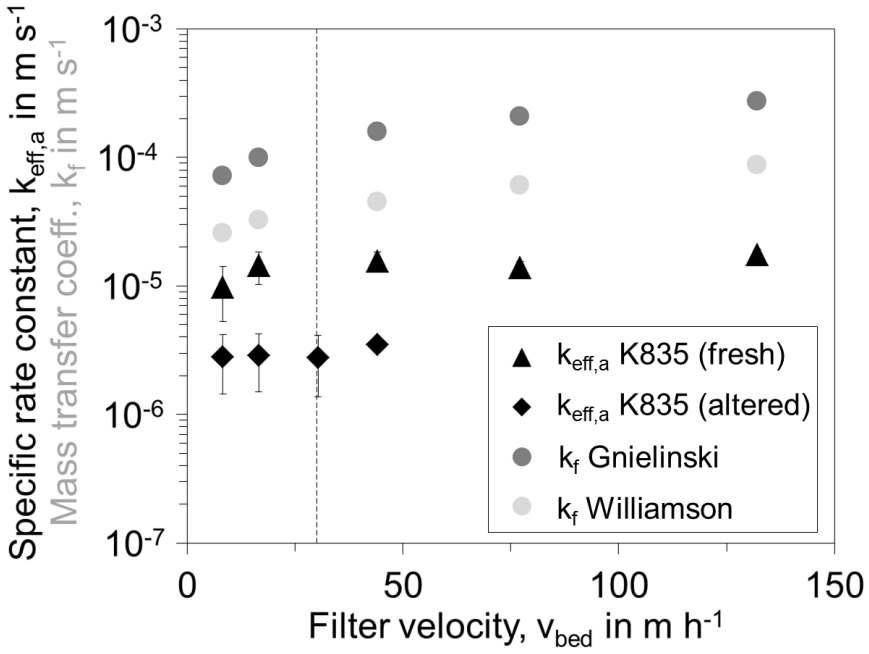

843

844 Figure 4: Impact of filter velocity on the experimentally determined apparent
845 surface related reaction rate constant $k_{app,a}$ for MCA conversion and
846 the theoretical mass transfer coefficient k_f of the unfractionated K835
847 GAC. Error bars represent the 95% confidence interval. Mass
848 transfer coefficients k_f were calculated using a mean grain diameter
849 $d_{hy,K835}$ of 1.39 mm. The dashed vertical line represents the
850 recommended filter velocity for GAC filters in swimming pool water
851 treatment in Germany (≤30 m h^{-1}) (DIN 19643-2, 2012).

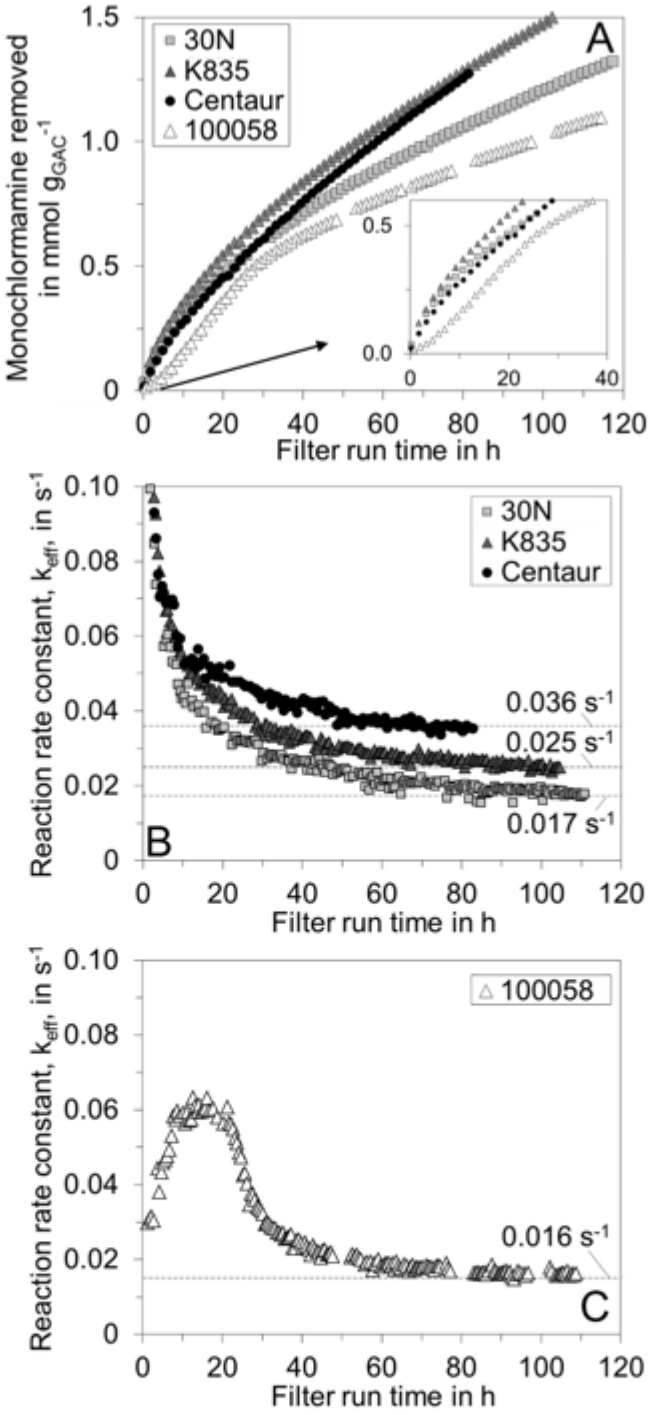

852

853 Figure 5: Removed MCA (A) and bed volume based apparent reaction rate

854 constant k_{app} for MCA removal (B, C) over the filter run time. All

855 GACs had the same grain size of ~0.55 mm (0.57 mm for the 100058

856 GAC). Dashed horizontal lines in (B) represent the GAC reactivity

857 when stationary conditions were reached.

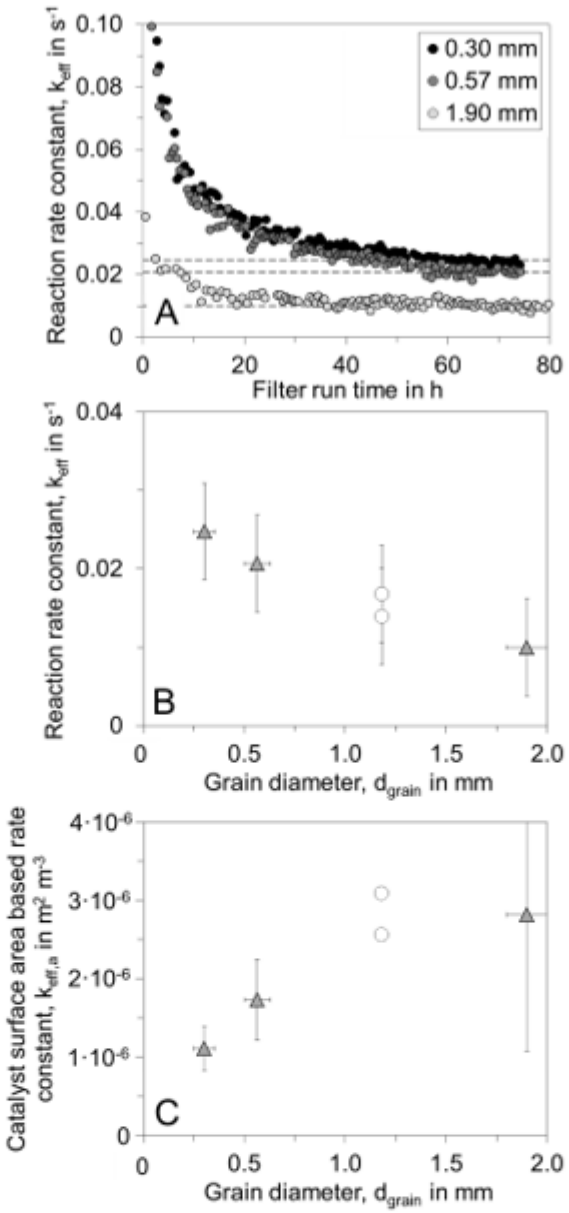

858

859 Figure 6: (A) Reaction rate constant k_{app} over the filter runtime for different

860 grain size fractions of the 30N GAC. Dashed horizontal lines

861 represent the level of GAC reactivity at stationary conditions. (B) k_{app}

862 and (C) $k_{app,a}$ at stationary conditions as function of the grain

863 diameter. Open circle symbols in (B) and (C) represent k_{app} for the

864 unfractionated 30N GAC using $d_{hy,30N}$ = 1.18 mm as representative

865 grain size (data not shown in A). Error bars in (B) and (C) represent

866 the 95% confidence intervals.

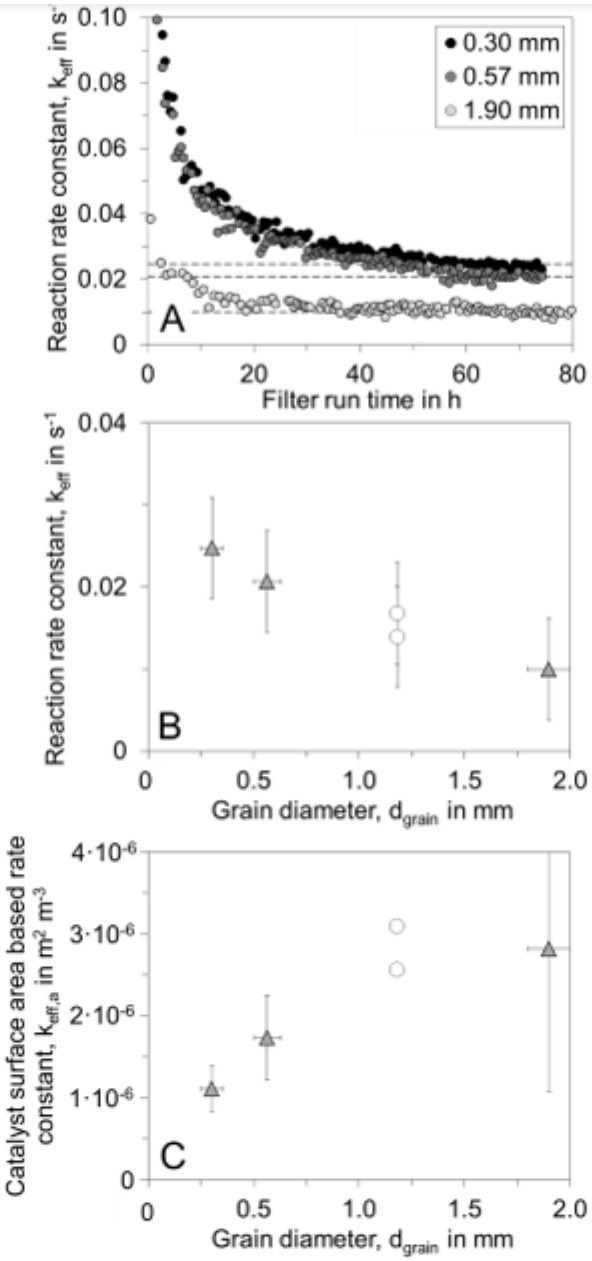

867

868 Figure 6: (A) Reaction rate constant k_{app} over the filter runtime for different

869 grain size fractions of the 30N GAC. Dashed horizontal lines

870 represent the level of GAC reactivity at stationary conditions. (B) k_{app}

871 and (C) $k_{app,a}$ at stationary conditions as function of the grain

872 diameter. Open circle symbols in (B) and (C) represent k_{app} for the

873 unfractionated 30N GAC using $d_{hy,30N}$ = 1.18 mm as representative

874 grain size (data not shown in A). Error bars in (B) and (C) represent

875 the 95% confidence intervals.

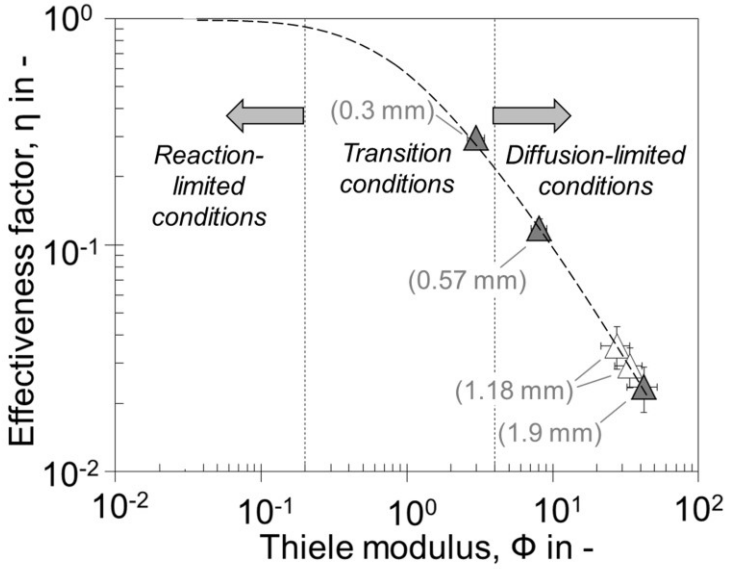

Figure 7: Effectiveness factor η of the MCA-GAC reaction at stationary conditions for different grain size fractions of the 30N GAC as function of the Thiele modulus Φ. Open triangle symbols represent k_{app} for the unfractionated 30N GAC using $d_{hy,30N}$ = 1.18 mm. Filled triangle symbols represent k_{app} for the fractionated 30N GAC. The dashed black line is for orientation only and represents the expected relationship between Φ and η as discussed elsewhere (Ertl et al., 1997). Error bars represent the 95% confidence intervals.

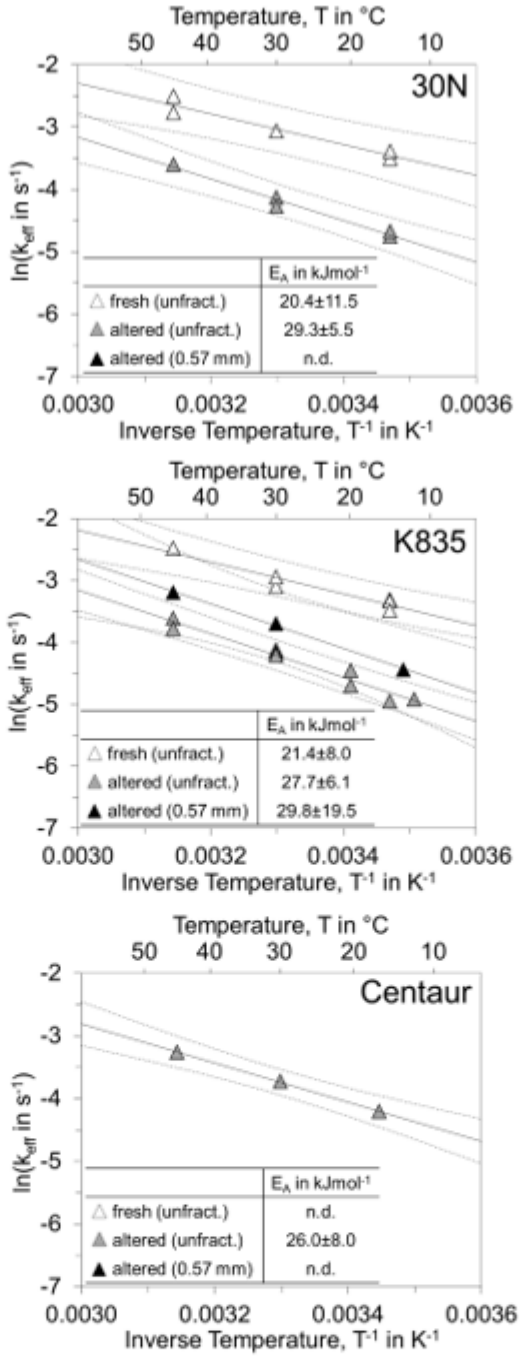

Figure 8: Impact of water temperature on the apparent reaction rate constant for MCA conversion at the GACs 30N, K835 and Centaur. Solid lines represent linear least-squares best fit and dashed lines represent the 95% confidence band of the regression. Errors for E_A represent the standard error of the slope of the linear regression (n = 3 - 6, depending on the carbon). (n.d. = not determined)

PORE DIFFUSION LIMITS REMOVAL OF MONOCHLORAMINE IN TREATMENT OF SWIMMING POOL WATER USING GRANULAR ACTIVATED CARBON

- Supplementary Material -

Bertram Skibinski[1*], Christoph Götze[1], Eckhard Worch[2], Wolfgang Uhl[1,3*]

[1] Technische Universität Dresden, Chair of Water Supply Engineering, 01062 Dresden, Germany.

[2] Technische Universität Dresden, Chair of Hydrochemistry, 01062 Dresden, Germany.

[3] Norwegian Institute for Water Research (NIVA), 0349 Oslo, Norway.

[*] Corresponding authors. E-mail address: wolfgang.uhl@niva.no
bertram.skibinski@tu-dresden.de

This PDF file includes:

3 Sections, 2 Figures, 1 Table and 5 Equations for further information.

A Additional information on the methods used for physical GAC characterisation

A.1 Specific outer surface area

The specific outer surface area a_o of the GAC bed was calculated based on the grain size distribution of the unfractionated GACs as follows:

$$a_0 = \frac{A_{bed}}{V_{bed}} = 6 \cdot \frac{\rho_{bed}}{\rho_{grain}} \cdot \sum_i \frac{q_i}{d_{grain,i}} \cdot \frac{1}{\psi} \quad (1)$$

Here ρ_{bed} and ρ_{grain} are the dry bed density and the dry density of the GAC grains, q_i is the mass fraction of the corresponding mean grain size $d_{grain,i}$ as derived from the grain size distribution, and ψ is the dimensionless non-sphericity correction factor, introduced in order to respect the deviation in shape of the GAC grains from a spherical form (ψ = 0,75 for GACs (Hawkslei, 1951). Grain size distributions of all GACs were analysed according to a German standard (DIN 66165-1, 1987) using a sieve tower (AS 200, Retsch, Germany). Results are given in section B.1 of the Supplementary information.

A.2 Bed and grain densities

ρ_{bed} and ρ_{grain} of the four GACs investigated were determined as follows: A volume of 25–35 mL of the respective GAC was soaked in a beaker with roughly 50 mL of deionised water. Vacuum was applied to remove air from the pores and to fill them with water. The grains were removed from the water and spread on a metal sieve gently shaken. Thus the GAC grain pores remained filled with water.

25 mL of deionised water (V_w) were placed in a 50 mL measuring cylinder and the mass noted. Then GAC grains with water-filled pores were slowly transferred from the metal sieve to the cylinder such that a bed of 15 mL (V_{bed}) was formed, after carefully consolidating the bed by manually tamping the measuring cylinder 15 times on a plate. The total volume of water with GAC grains in the measuring cylinder was denoted as V_{w+GAC}. The mass of the water and the grains was noted as m_{w+GAC}.

The volume of the wet GAC grains was:

$$V_{GAC(wet)}=V_{w+GAC}-V_w \quad (2)$$

Subsequently, the GAC suspension was taken from the cylinder and spread over a filter paper of mass m_{fil}. The filter paper with GACs was dried at 110 °C for ~24 h until the weight of the filter paper reached constancy and no water remained in the pores of the GAC grains. The mass of the dry filter paper with GAC grains was denoted as $m_{fil+GAC}$. The mass of the dry GAC grains m_{grain} was calculated as the difference between $m_{fil+GAC}$ and m_{fil}.

According to the procedure, then bed density (dry) ρ_{bed} of the GAC bed is given by

$$\rho_{bed}=\frac{m_{grain}}{V_{bed}} \quad (3)$$

The density of the GAC grains (dry) ρ_{grain} is given by

$$\rho_{grain}=\frac{m_{grain}}{V_{GAC(wet)}} \quad (4)$$

ρ_{bed} and ρ_{grain} are given as average obtained from three determinations.

A.3 Hydraulic diameter

The representative hydraulic grain size d_{hy} of the unfractionated GACs was calculated from the grain size distribution as follows (Kozeny, 1927):

$$d_{hy} = \frac{1}{\sum\left(\frac{q_i}{d_{grain,i}}\right)} \quad (5)$$

A.4 Internal surface area and pore volumes

The internal surface area, the pore volume of micropores and mesopores, the pore size distribution (PSD) and the tortuosity of the fresh unfractionated GACs were determined from nitrogen adsorption/desorption isotherms. Nitrogen adsorption/desorption isotherms were determined in a relative pressure range (p/p_0) of 10^{-6} to 1 at 77 K using an automated gas-sorption apparatus (Autosorb-1C, Quantachrome, Germany). The internal surface area of the GACs was determined using the BET equations (Brunauer et al., 1938). The total pore volume was calculated from the nitrogen sorption data at p/p_0 of ~0.98 while the micropore volume was determined using the Dubinin-Radushkevich equation at p/p_0 of 10^{-6} - 10^{-1}. For calculations, ASiQWin Software (Version 3.0, Quantachrome Instruments) was used. The sum of mesopore (2 – 50 nm) and macropore (>50 nm) volume was calculated by subtracting the micropore (<2 nm) volume from the total pore volume. N_2 adsorption-desorption isotherms were further used to estimate the tortuosity of the GACs using the CSTM-model as described previously (Salmas and Androutsopoulos, 2001) (see Table 2).

The surface area and pore size distribution (PSD) of the GACs were determined using the quenched solid density functional theory (QSDFT) assuming graphite

material with pores of slit-like shape (Neimark et al., 2009). The validity of this assumption is discussed in Section 3.2. The proportion of macropores (>50 nm) was determined by mercury intrusion porosimetry using a Porosimeter 2000 apparatus (Carlo Erba Instruments, Milan, Italy). The intrusion experiments were performed in a pressure range of 0.4 to 200 MPa.

Images of the 100058 GAC were made with a High Resolution Scanning Electron Microscope (HRSEM) (FEI Nova NanoSEM, 5 kV) and were taken at four different positions across the grain radius. In total, six close-up HRSEM images of each position across the diameter were taken. The pore size distribution of the 100058 GAC across the grain diameter was analysed by image processing of the close-up HRSEM-images as described previously by the authors (Skibinski et al., 2016). Due to the limited resolution of the HRSEM-images, only pores >10 nm could be analysed.

B Additional results of the physical GAC characterisation

B.1 Grain Size Distributions

The distributive grain size distribution is shown in Figure B.1 and cumulative grain size distribution of the GACs is shown in Figure B.2.

The specific outer surface areas, densities and hydraulic diameters are summarised in Table 1.

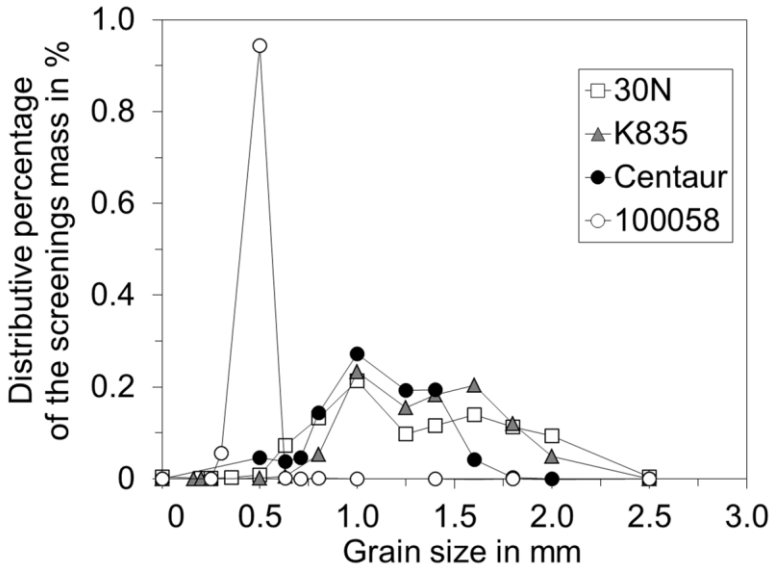

93

94 Figure B.1: Distributive grain size distribution of the fresh unfractionated GACs

95 30N, K835, Centaur and 100058.

96

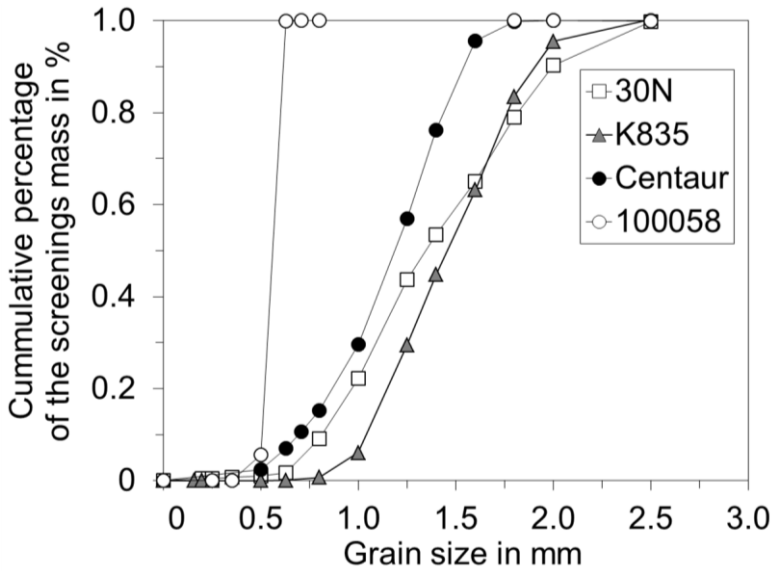

97

98 Figure B.2: Cumulative grain size distribution of the fresh unfractionated GACs

99 30N, K835, Centaur and 100058.

Table B.1: Hydraulic diameter d_{hy}, bulk density (dry) ρ_{bed}, density of the GAC grains ρ_{grain} and specific outer surface area a_o of the fresh unfractionated GACs 30N, K835, Centaur and 100058.

GAC type	d_{hy} in mm	ρ_{bed} **in g mL^{-1}**	ρ_{grain} **in g mL^{-1}**	a_o **in m² m^{-3}**
30N	1.18	0.47	0.56	5444
K835	1.39	0.59	0.76	4480
Centaur	1.00	0.50	0.77	5532
100058	0.55	0.72	0.60	17418

B.2 Pore Size Distributions

Figure B.3 shows the N_2 adsorption-desorption isotherms of the fresh unfractionated GACs and the corresponding pore size distribution (PSD). The N_2 adsorption-desorption isotherms were type I according to the Brunauer-Deming-Deming-Teller (BDDT) classification for all GACs considered. The total internal surface area (BET surface) for all GACs ranged between 895 and 1291 m² g_{GAC}^{-1} (see Table 2) and was in accordance with data found in the literature. The sharp increase of N_2 adsorption in the low pressure region indicates the presence of plentiful micropores (Brunauer et al., 1940). The percentage of micropores with regard to the total pore volume is shown in Table 2. The relative proportion of mesopores was the highest for 100058 (18 %) and Centaur (17 %) GACs. The hysteresis of nitrogen physisorption (the difference between adsorption and desorption isotherms) for the 30N and K835 GACs was almost zero. The fact that adsorption and desorption isotherms branch in parallel to each other and almost horizontally is associated with the presence of narrow pores of slit-like shape, which are commonly found for activated GACs (Hu et al., 2001).

In the micropore region (<2 nm), the Centaur, K835 and 100058 GAC showed PSD peaks at the smallest detectable pore size of 0.6 nm and at ~1.1 nm. Both Centaur and K835 GACs showed a PSD peak at 1.1 nm, while the 30N GAC showed peaks at 0.72 and 1.5 nm. The characteristic pore size distribution of the Centaur GAC is in agreement with data reported previously (Bashkova et al., 2007). Both the Centaur and the 100058 GACs contained a significant proportion of large mesopores of >7 nm (0.015 $cm^3 g^{-1}$ (Centaur) and 0.013 $cm^3 g^{-1}$ (100058)). Mercury intrusion porosimetry measurements showed that the proportion of macropores (macropore volume related to the total pore volume) was very low and ranged between 1.6 and 3.6 %.

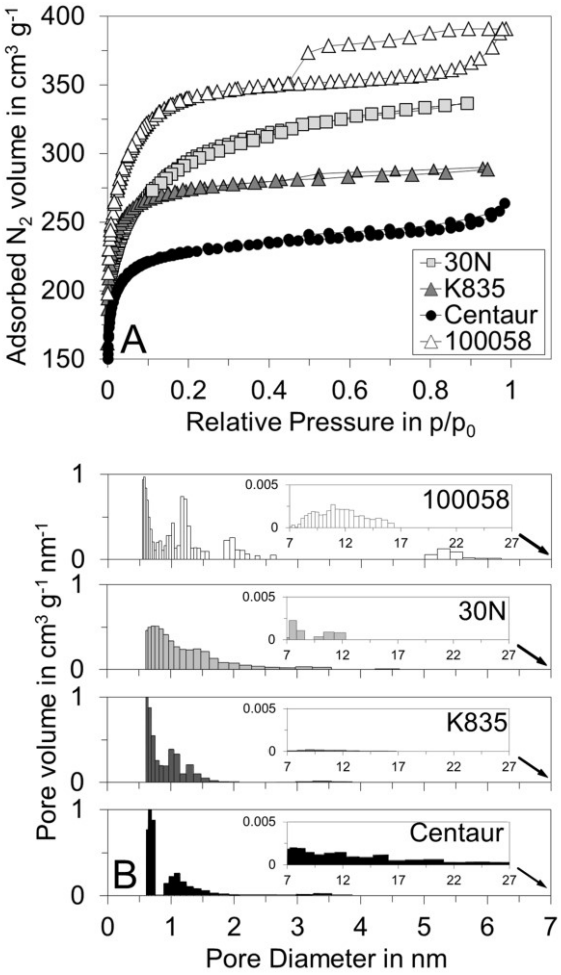

Figure B.3: N_2 adsorption and desorption isotherms at 77 K (A) and pore size distribution of the unfractionated fresh GACs (B) (inset represents the distribution of large mesopores of >7 nm).

B.3 Characterisation of the ordered pore size distribution of the 100058 GAC

Examples of close-up HRSEM images of the 100058 GAC taken at different positions across the radius of a cross-section are presented in Figure B.4. It revealed that the obvious textural change across the diameter of the grain (Figure B.4(A)) is accompanied by a change in the pore size distribution (Figure B.4(B-D)). From the relative pore size distribution it becomes obvious that plenty of mesopores are present at the outer region of the grain, while their relative proportion decreases

141 towards the centre of the grain. Near of the centre of a grain (position D), no
142 macropores were present and mesopores revealed a mean diameter of ~25 nm.

143 No structural changes were revealed from the HRSEM images of the K835 (D1), 30N
144 (D2) and Centaur (D3) carbon, supporting the assumption of an equal pore size
145 distribution proposed for the three GACs by earlier studies (Radian et al., 2011;
146 Aleghafouri et al., 2012; Bashkova et al., 2007).

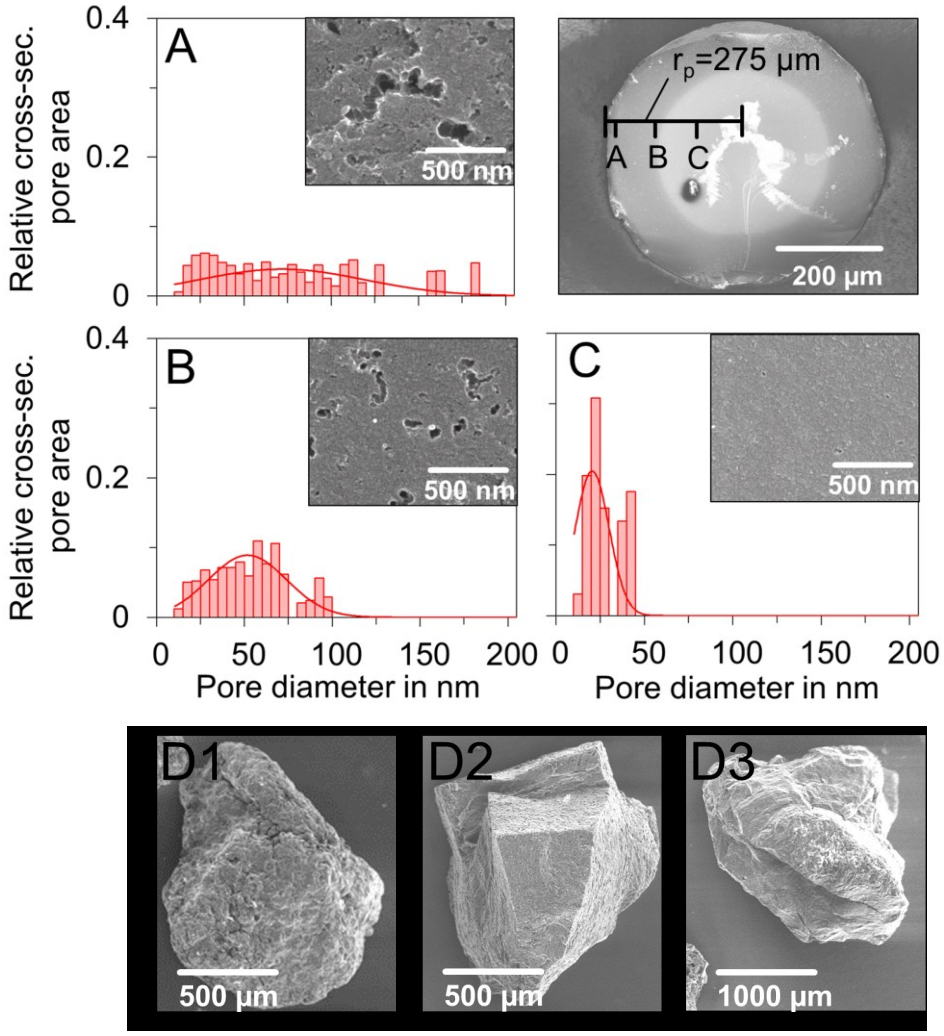

Figure B.4: HRSEM image of a cross-section of the 100058 GAC at a zoom of 150 (top right) and at different positions across the diameter with the corresponding relative cross-sectional pore area distribution at a zoom of 200,000 (A-C). Further, HRSEM images of the K835 (D1), 30N (D2) and Centaur (D3) GACs are shown at a zoom of 50 (D1, D2) and 21 (D3). Solid lines in (A-C) represent the log-normal distribution.

C Additional information on the GAC's conversion–time behaviour

The difference in conversion–time behaviour between the microporous GACs (K835, 30N and Centaur) and the 100058 GAC can be explained by the unusual pore size distribution of the latter, as follows:

(i) Due to the high proportion of mesopores near to the external surface of the grains of the 100058 GAC (Figure 3(B)), the effective diffusion coefficient of monochloramine ($D_{E,MCA}$) in this area is high and the overall reaction is controlled by the intrinsic chemical reaction at the beginning.

(ii) The observed decrease in mean pore size towards the centre of the grains of the GAC 100058 will lead to an increase of the accessible pore area reached by the reaction front when moving towards the centre. As a result, the reactivity of the 100058 GAC increases during the first ~20 min of the reaction.

(iii) With on-going reaction time, the reaction front moves further towards the grain's centre and diffusion paths of monochloramine molecules increase until a shift in the reaction controlling mechanism from chemical control to diffusional control occurs. This shift results in a decrease in reactivity, which in turn leads to a sigmoid conversion time curve (Levenspiel, 1999), as was found for the 100058 GAC.

In contrast to the 100058 GAC, the pore structure of the conventional GACs (30N, K835, Centaur) is assumed to be microporous throughout the entire particle. Thus,

for those GACs the overall process is controlled by diffusion right from the start of the reaction, leading to hyperbolic conversion–time curves (Levenspiel, 1999).

References

Aleghafouri, A., Mohsen-Nia, M., Mohajeri, A., Mahdyarfar, M., Asghari, M., 2012. Micropore size analysis of activated carbons using nitrogen, carbon dioxide and methane adsorption isotherms: Experimental and theoretical studies. Adsorption Science and Technology 30, 307-316.

Bashkova, S., Baker, F.S., Wu, X.X., Armstrong, T.R., Schwartz, V., 2007. Activated carbon catalyst for selective oxidation of hydrogen sulphide: On the influence of pore structure, surface characteristics, and catalytically-active nitrogen. Carbon 45, 1354-1363.

Brunauer, S., Emmett, P.H., Teller, E., 1938. Adsorption of gases in multimolecular layers. Journal of the American Chemical Society 60, 309-319.

Brunauer, S., Deming, L.S., Deming, W.E., Teller, E., 1940. On a theory of the van der Waals adsorption of gases. Journal of the American Chemical Society 62, 1723-1732.

DIN 66165-1, 1987. Particle size analysis - Sieve analysis, Part1: Fundamentals (in German: Partikelgrößenanalyse – Siebanalyse, Teil 1: Grundlagen). Normenausschuß Siebböden und Kornmessung (NASK) im DIN Deutsche Institut für Normung. Beuth Verlag, Berlin.

Hawkslei, P.G.W., 1951. The physics of particle size measerment: Part I. Fluid dynamics and the Stokes diameter. British Coal Utilisation Research Association 15, 105-146.

Hu, Z.H., Srinivasan, M.P., Ni, Y.M., 2001. Novel activation process for preparing highly microporous and mesoporous activated carbons. Carbon 39, 877-886.

Kozeny, J., 1927. Über kapillare Leitung des Wasers im Boden (in German). Akademie der Wissenschaften Wien, 271–306.

Levenspiel, O., 1996. The Chemical Reactor Omnibook. OSU Book Stores Inc., Corvallis.

Neimark, A.V., Lin, Y.Z., Ravikovitch, P.I., Thommes, M., 2009. Quenched solid density functional theory and pore size analysis of micro-mesoporous carbons. Carbon 47, 1617-1628.

Radian, A., Carmeli, M., Zadaka-Amir, D., Nir, S., Wakshal, E., Mishael, Y.G., 2011. Enhanced removal of humic acid from water by micelle-montmorillonite composites: Comparison to granulated activated carbon. Applied Clay Science 54, 258–263.

Salmas, C.E., Androutsopoulos, G.P., 2001. A novel pore structure tortuosity concept based on nitrogen sorption hysteresis data. Industrial and Engineering Chemistry Research 40, 721-730.

Skibinski, B., Mueller, P., Uhl, W., 2016. Rejection of submicron sized particles from swimming pool water by a monolithic SiC microfiltration membrane: Relevance of steric and electrostatic interactions. Journal of Membrane Science 499, 92-104.